

AD-781 840

AN ANALYSIS OF THE POSITIONING ACCURACY
OF HORIZONTAL SEXTANT ANGLES

John T. Tozzi, et al

U.S. Coast Guard
Washington, D. C.

June 1974

DISTRIBUTED BY:

NTIS

National Technical Information Service
U. S. DEPARTMENT OF COMMERCE
5285 Port Royal Road, Springfield Va. 22151

This document is disseminated under the sponsorship of the Department of Transportation in the interest of information exchange. The United States Government assumes no liability for its content or use thereof.

The contents of this report do not necessarily reflect the official view or policy of the Coast Guard, and they do not constitute a standard, specification or regulation.

This report, or portions thereof, may not be used for advertising, publication, or promotional purposes. Citation of trade names and manufacturers does not constitute endorsements or approval of such products.

ACCESSION for	
NTIS	Whi's Section <input checked="" type="checkbox"/>
D.C.	But. Section <input type="checkbox"/>
UNAL. PENDING	<input type="checkbox"/>
JUSTIFICATION	
BY	
DISTRIBUTION/AVAILABILITY CODES	
Dist.	AVAIL. and/or SPECIAL
A	

G. J. Budridge
G. J. BUDRIDGE
Commander, U. S. Coast Guard
Acting Chief, Environmental and
Transportation Technology Division
Office of Research and Development
U. S. Coast Guard Headquarters
Washington, D. C. 20590

1. Report No. CG-D-106-74	2. Government Accession No.	3. Recipient's Catalog No. AD 781840	
4. Title and Subtitle An Analysis of the Positioning Accuracy of Horizontal Sextant Angles		5. Report Date June 1974	
		6. Performing Organization Code	
7. Author(s) LT John T. Tozzi, USCG and LT Harold E. Millan, USCG		8. Performing Organization Report No.	
9. Performing Organization Name and Address		10. Work Unit No. (TRAIS)	
		11. Contract or Grant No.	
		13. Type of Report and Period Covered Final Report Oct. 1973 - Mar. 1974	
12. Sponsoring Agency Name and Address Office of Research and Development U. S. Coast Guard Washington, D. C. 20590		14. Sponsoring Agency Code	
15. Supplementary Notes			
16. Abstract <p>Horizontal sextant angles is the primary buoy anchor positioning method used by the U. S. Coast Guard today. Interest in the accuracy capabilities of this technique has been spurred by the increased channel-marking accuracy requirements of the ever-growing population of very large merchant vessels. This paper presents a method for determining the positioning accuracy which may be obtained from horizontal sextant angle fixes.</p> <p>A system model for a three-object, two-line-of-position (LOP) fix is developed from which the independent and dependent component instrument and human factors errors for both the sextant and the three-arm protractor can be identified and analyzed. The conversion of these angular measurement errors into distance units is accomplished by a function termed the Geometric Multiplication of Precision (GMOP) which is derived from the gradient of β (β is defined as the exact angular measurement of a horizontal sextant angle). The LOP errors in distance units are used with the LOP crossing angle to determine the positioning accuracy, expressed as the radius from the exact position within which the actual position may be expected to lie for a particular accuracy probability.</p> <p style="text-align: center;">reproduced by NATIONAL TECHNICAL INFORMATION SERVICE U.S. Department of Commerce Springfield, VA 22151</p>			
17. Key Words Buoy Positioning, Horizontal Sextant Angles, Triangulation, Error Analysis, Positioning Accuracy		18. Distribution Statement Document is available to the public through the National Technical Information Service, Springfield, Virginia 22151	
19. Security Classif. (of this report) Unclassified	20. Security Classif. (of this page) Unclassified	21. No. of Pages 103	22. Price

****PREFACE****

This report presents the results of an independent investigation into the accuracy of horizontal sextant angles as a method of establishing geographic position conducted by the authors from October 1973 to March 1974. It includes a description of the system, the development of a method for determining positioning accuracy and an example problem with a step-by-step procedure for utilizing the developed method. Supporting theory, analysis and proofs are included wherever possible for the convenience of the reader.

****ACKNOWLEDGEMENTS****

The authors wish to extend their sincere thanks to MARY E. TOZZI for her perseverance through the many hours of tedious typing.

TABLE OF CONTENTS

PREFACE	3
ACKNOWLEDGEMENTS	4
LIST OF FIGURES	7
NOTATION	9
SUMMARY	13
INTRODUCTION	16
1. HORIZONTAL SEXTANT ANGLES AS A POSITIONING METHOD	18
1.1 Theoretical Basis	18
1.2 Practical Application	22
1.3 Sources of System Error	26
2. POSITIONING ACCURACY	30
2.1 Preliminary Considerations	30
2.2 The Probability Theory	33
2.3 The Basic Method	35
3. THE GEOMETRIC MULTIPLICATION OF PRECISION (GMOP)	46
3.1 The Role of the GMOP	46
3.2 The Mathematical Expression for an LOP	47
3.3 The Derivation of the GMOP	50
3.4 The Nature of the GMOP	51
3.5 The Feasibility of Linear Interpolation for GMOP	55
4. THE LOP CROSSING ANGLE (α)	63
4.1 The Calculation of α	63

5.	AN EXAMPLE PROBLEM	71
5.1	The General Procedure	71
5.2	Probabilistic Variable Definitions	76
5.3	The Actual Problem	79
	REFERENCES	83
	APPENDIX A	84
	APPENDIX B	90
	APPENDIX C	101
	APPENDIX D	104

LIST OF FIGURES

Fig. 1-1	Typical triangle OPQ showing circumscribing circle	19
Fig. 1-2	Different triangles with common side OQ and the same circumscribing circle	19
Fig. 1-3a	Isosceles triangle OPQ from Fig. 1-2	21
Fig. 1-3b	Triangle OP'Q from Fig. 1-2	21
Fig. 1-4	Geometric situations resulting from two-LOP horizontal sextant angle fixes	24
Fig. 1-5	Horizontal sextant angle description	28
Fig. 2-1	Expanded view of intersection of two lines of position	32
Fig. 2-2	Contours of constant β (circular LOP's)	32
Fig. 2-3	Conversion of probability ellipse to circle	44
Fig. 3-1	The relationship between contours of constant β and $\nabla\beta$ curves	48
Fig. 3-2	Circular LOP showing pertinent parameters	48
Fig. 3-3	Circular LOP's showing points M_β of maximum GMOP	54
Fig. 3-4a	Curves of GMOP vs. ϵ for $\beta = 5^\circ, 10^\circ, 25^\circ$	56
Fig. 3-4b	Curves of GMOP vs. θ for $\beta = 45^\circ, 65^\circ, 85^\circ, 105^\circ, 125^\circ$	57
Fig. 3-5	Contours of constant GMOP drawn to scale (baseline OQ of length A)	58
Fig. 3-6	$-\frac{\partial \text{GMOP}}{\partial \beta} \Big _\theta$ vs. β for incremental θ	60
Fig. 3-7	$\frac{\partial \text{GMOP}}{\partial \theta} \Big _\beta$ vs. θ for incremental β	61
Fig. 4-1	Illustration of LOP crossing angles for the two general geometric cases of Fig. 1-4	64

Fig. 4-2	One LOP showing the angle ψ	65
Fig. 4-3	Geometric situations near the intersection of the LOP's for Fig. 4-1a	66
Fig. 4-4	Geometric situations near the intersection of the LOP's for Fig. 4-1b	68
Fig. 4-5	A swing angle ($\alpha = 0$)	70
Fig. 5-1	Portion of C & GS Chart #220 showing buoy and fixed objects for example problem	80
Fig. A-1	The error in placing arm PQ through the center of Q	85
Fig. A-2	The errors affecting β_1 due to the incorrect placement of pivot point over P	85
Fig. A-3	Defining the angular changes Δk_1 and $\Delta \theta_1$	88
Fig. A-4	Defining the angular changes $\Delta \theta_2$ and Δk_2	88
Fig. B-1	Reconstruction of Fig. 1-3a showing additional angular and linear measurements	91
Fig. B-2	Graphic representation of Eq. B.5 for $0 \leq \beta \leq 5^\circ$	91
Fig. B-3	Graphic representation of Eq. B.20 for $0 \leq \beta \leq 5^\circ$	100

NOTATION

A	The baseline length, OQ for LOP-1 and QQ' for LOP-2 (fig. 3-2)
C	The center of a circular LOP
E_1, E_2	Dependent orthogonal coordinates into which the actual LOP errors ϵ_1 and ϵ_2 are transformed (Section 2.3)
GMOP	The Geometric Multiplication of Precision, $\frac{\hat{K}}{A}$ (eq. 3.1)
K	The factor obtained from fig. 2-3 which is used in eq. 2.36 to determine R
\hat{K}	The factor which converts small angular changes in β (radians) into distance units (eq. 2.21)
\tilde{K}	A constant used in the analysis of Appendix B
O	The left-hand fixed object when viewing from the fixed objects to the observers' position (figs. 1-4)
P	The observers position (figs. 1-4)
Q	The center fixed object (figs. 1-4)
Q'	The right-hand fixed object when viewing from the fixed objects to the observers' position (figs. 1-4)
R	The radius of the circular probability contour from the exact position within which the actual position may be expected to lie
\hat{R}	The radius of a contour of constant β (a circular LOP) (fig. B-1)
\tilde{R}	The radius of a $\tilde{\nabla}\beta$ curve
\hat{r}	A unit vector in the r direction in the polar coordinate system
r	The distance from a fixed object to P (figs. A-3 and A-4); also, the magnitude of the \hat{r} vector in the polar coordinate system (fig. 3-2)

s', t, u	Measurable distance errors in placing the three-arm protractor pivot point directly over the desired position which are used to determine $\Delta\theta_1$, $\Delta\theta_2$ and $\Delta\kappa_2$ (figs. A-3 and A-4)
x, y	The independent orthogonal coordinates into which E_1 and E_2 are transformed (Section 2.3); also the variables of the Cartesian coordinate system (Appendix B)
y	The magnitude of the \vec{y} vector constructed from the exact three-arm protractor arm position to the actual arm position, perpendicular to the exact position at the fixed object (fig. A-1)
α	The angle of intersection of the LOP's (crossing angle); always an acute angle (fig. 4-1)
β	The exact measurement of the horizontal sextant angle to be observed; sometimes subscripted to indicate LOP reference
ϵ	An angular error in the measurement of the horizontal sextant angle; usually subscripted to indicate the source of the error (Section 1.3, Section 2.3, Appendix A)
f	The angle through which the dependent orthogonal E_1 and E_2 coordinate axes are rotated to yield the independent orthogonal x and y coordinate axes (Section 2.3)
η	The angle POC and the angle OPC used in the derivation of α in Section 4.1 (fig. 4-2)
θ	The angle POQ for LOP-1 and angle PQQ' for LOP-2; sometimes subscripted to indicate LOP reference (fig. 4-1)
$\hat{\theta}$	A unit vector in the θ direction in the polar coordinate system
$\Delta\theta$	The change in θ due to the misplacement of the three-arm protractor pivot point (figs. A-3 and A-4); usually subscripted to indicate LOP reference
κ	The angle PQO for LOP-1 and angle PQ'Q for LOP-2; usually subscripted to indicate LOP reference (figs. A-3 and A-4)
$\Delta\kappa$	The change in κ due to the misplacement of the three-arm protractor pivot point (figs. A-3 and A-4); usually subscripted to indicate LOP reference

μ	The covariance of two dependent random error variables in angular units (eq. 2.14); usually subscripted to indicate LOP reference
μ_d	The covariance of two dependent random error variables in distance units (eq. 2.28)
ρ	The correlation coefficient of two random error variables (eq. 2.13)
σ	The standard deviation of a particular random error distribution in angular units (the square root of σ^2); usually subscripted to indicate LOP reference
σ_d	The standard deviation of a particular random error distribution in distance units (the square root of σ_d^2)
σ^2	The variance of a particular random error distribution in angular units (eq. 2.8)
σ_d^2	The variance of a particular random error distribution in distance units (eqs. 2.23 and 2.24)
ϕ	A quantity which is constant on a particular $\nabla\beta$ curve (Appendix B)
ψ	The angle between r_1 or r_2 and a tangent to LOP-1 or LOP-2, respectively, measured as shown in fig. 4-2.

SUMMARY

The text is preceded by a brief introduction which outlines the history of horizontal sextant angles as a positioning method, the reason for the recent interest in defining the accuracy of the system and the general direction of the analysis which follows. The description of the method of horizontal sextant angles as a means of establishing geographic position, including the theoretical basis for its use and an illustration of a particular method of utilization, is contained in Chapter 1. A general description of the instruments used is included also. Chapter 1 ends with the development of the error model describing each of the component dependent and independent angular errors which affect an exact angular measurement. Errors in the use of both the three-arm protractor and the sextant are considered. The error model is used in Chapter 2 to develop the basic method for determining positioning accuracy.

The development of the basic method for determining positioning accuracy is begun with an explanation of the necessary mathematical considerations and a brief look at the applicable probability theory. The steps in the actual development include:

1. The definition of the individual LOP (line of position) variances and the combined LOP covariance from the component angular errors.
2. The conversion of the variances and the covariance to distance units.
3. The elimination of the dependence of the LOP errors using Fraser's method (ref. 3).

Preceding page blank

4. The determination of the radius of the circular probability density contour within which the actual position can be expected to lie.

The Geometric Multiplication of Precision (GMOP) is derived and analyzed in Chapter 3. The GMOP is defined as a dimensionless quantity \hat{R} per unit baseline length, where \hat{K} is the conversion factor used to obtain the LOP variances and covariance in distance units. (The conversion is from radians to distance units.) The similarity between the characteristics of the gradient of β (β is defined as the exact angular measurement of a horizontal sextant angle) and the desired traits of the GMOP sets the direction of the development toward finding GMOP as a function of $\text{grad } \beta$. The equation of β in the polar coordinate system is found, and the GMOP is derived as the reciprocal of the magnitude of $\text{grad } \beta$. The GMOP is analyzed thoroughly to investigate its physical correlation and its functional behavior.

Chapter 4 contains the derivation of a simple method for determining the LOP crossing angle α . This quantity is required for the implementation of the basic method described in Chapter 2. It is shown that α is easily obtainable from the measurable quantities which are required for the calculation of the GMOP.

Chapter 5 presents an example problem for the convenience of the reader with a step-by-step procedure for applying the total method to a practical situation. The lack of suitable published human factors data for the three-arm protractor and the sextant forces certain assumptions concerning the statistical distributions of the component

angular errors. All assumptions are explained before the problem solution is presented.

Appendix A offers the methods of obtaining the component angular error distributions for the human factors errors in using the three-arm protractor from measurable distance errors in placing the pivot point and the arms. These methods can be applied to suitable experimental data to obtain the component angular error distributions from which the probabilistic variables necessary for the implementation of the method for determining positioning accuracy are derived.

Appendix B contains the proof of the acceptability of the LOP-error model of fig. 2-1. Specifically, the contention that, in the neighborhood of the observers' position, the LOP's approximate straight lines and the grad β curves along which the error is measured are essentially straight lines perpendicular to the exact and the error LOP's is proven to be reasonable. Appendices C and D show some intermediate steps for derivations contained in Chapter 3.

INTRODUCTION

The advantages in convenience and precision of using horizontal angles for finding a position on land was recognized certainly before the seventeenth century. The application of the method to hydrographic surveys and shipboard navigation was delayed considerably due to the lack of a suitable angle measuring instrument. The invention of the octant by John Hadley in 1731 provided such an instrument for marine use, and the Rev. John Michell suggested the use of the octant for triangulation afloat in 1765.⁸

Since the time of Hadley and Michell, the application of horizontal sextant angles to marine positioning problems which require great precision has increased markedly. One specific application for which the method is suited well is buoy anchor positioning. The U. S. Coast Guard maintains more than 20,000 floating aids to navigation which mark navigable channels and hazards to navigation in the waters of the United States. The Coast Guard Aids to Navigation Manual (CG-222) prescribes horizontal sextant angles as the primary buoy anchor positioning method to be used by U. S. Coast Guard buoy tenders. Interest in the accuracy of this positioning method has been spurred within the Coast Guard by the growing population of very large merchant vessels whose requirements for accurate channel marking are emphasized by the extremely severe consequences of grounding, e.g., cargo loss, ecological catastrophe and vessel damage.

A method for determining the accuracy which can be expected for a particular horizontal sextant angle position fix is derived and presented

in this report. Chapter 1 offers the theoretical basis for using horizontal sextant angles as a positioning method and the development of the system model for a three-object, two-line-of-position fix. The basic method is developed from a random error analysis in Chapter 2. Chapters 3 and 4 and Appendix A contain supporting derivations which provide necessary inputs to the basic method of Chapter 2. An example problem is presented in Chapter 5 for the convenience of the reader to demonstrate the application of the total method to a practical situation, including a step-by-step procedure which facilitates the calculations.

1. HORIZONTAL SEXTANT ANGLES AS A POSITIONING METHOD

1.1 Theoretical Basis

The utility of horizontal sextant angles as a means of establishing geographic position (called position fixing) is based upon the following geometric principles:

- a. Any three points in space are coplanar and define a circle whose orientation and dimensions depend upon the relative positions of the three points.
- b. Consider a circle with two fixed points on its circumference which are connected by a chord. The angle formed by the line segments constructed from each of the two fixed points to any point P on the circumference is constant for all points P in the same segment of the circle. (A segment of a circle is that portion of the circle which is bounded by an arc and its chord.)

The fact that any three points in space define a plane is basic and will not be justified further herein. The proof of the second part of principle "a" is founded upon the equidistance of all the points on the circumference of a circle from its center. Fig 1-1 shows a typical triangle OPQ. The perpendicular bisectors of OQ and OP, labeled WX and YZ respectively, are shown also. The end points of the bisected segments are equidistant from any particular point on the perpendicular bisector. Therefore, O and Q are equidistant from any particular point on WX; and O and P are equidistant from any particular point on YZ. It follows that

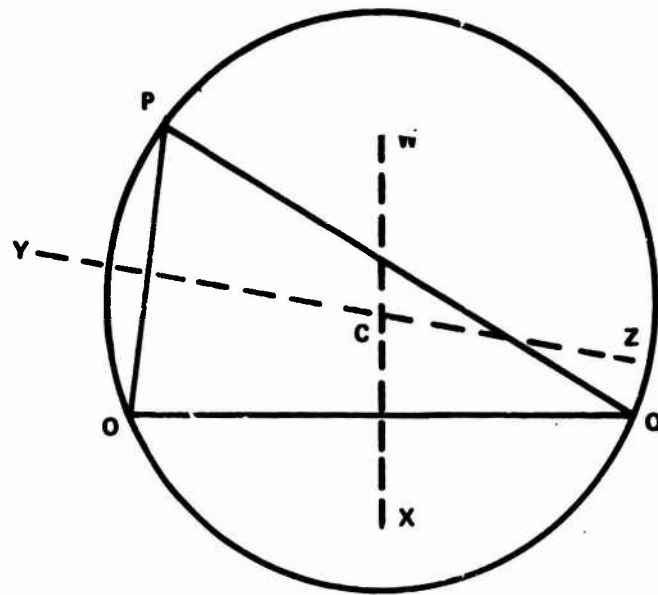


FIG. 1-1 TYPICAL TRIANGLE OPQ SHOWING CIRCUMSCRIBING CIRCLE

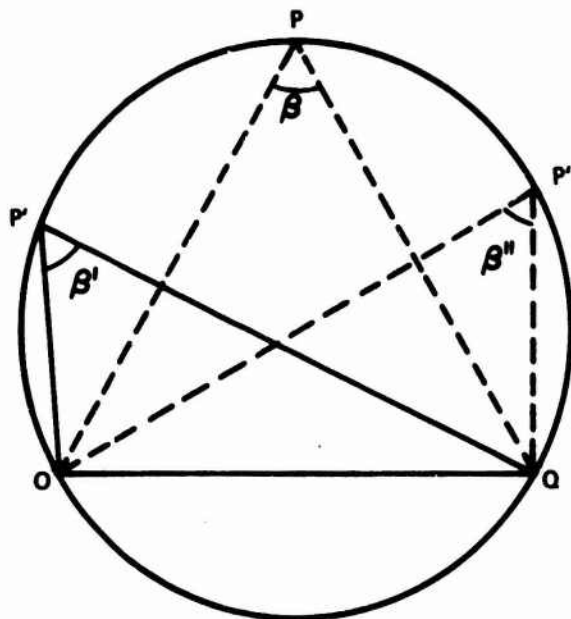


FIG. 1-2 DIFFERENT TRIANGLES WITH COMMON SIDE OQ AND THE SAME CIRCUMSCRIBING CIRCLE

O, P and Q are equidistant from the point of intersection of WX and YZ, labeled C. Consequently, O, P and Q are on the circumference of a circle whose center is C. Further, since WX and YZ are straight lines, they intersect at only one point; so only one circle is defined by O, P and Q.

The contention of principle "b" is illustrated in fig 1-2. If O and Q are fixed on the circumference of the circle, the value of the angle formed by line segments OP and QP is constant for all points P in the same segment of the circle, i.e., $\beta = \beta' = \beta''$. Fig 1-3a depicts the situation when the lengths of OP and QP are equal (OPQ is an isosceles triangle). The isosceles triangle OCQ, whose sides are the baseline OQ and the radii CO and CQ, is shown also. (The standard symbols Δ for triangle and \angle for angle will be used henceforth.) Now, the line segment PS is constructed as the perpendicular bisector of OQ, which is the base of ΔOPQ and a chord of the circle. Consequently, PS passes through C and bisects $\angle OPQ$. Therefore, $\angle OPC = \angle OPS = \beta/2$; and, since ΔOPC is also isosceles, $\angle POC = \angle OPC$. It follows that $\angle OCP = \pi - \beta$ and $\angle OCS = \beta$. This implies that $\angle COQ = \frac{\pi}{2} - \beta$. Fig 1-3b shows another possible configuration of the inscribed triangle. Again, O and Q are the fixed points on the circumference of the same circle; but this time the triangle is defined by O, P' and Q. The triangles OCQ of figs 1-3a and 1-3b are identical. Since $\angle COQ = \frac{\pi}{2} - \beta$, from fig 1-3b,

$$\angle P'OC = \theta - \angle COQ = \theta + \beta - \frac{\pi}{2} \therefore \angle OP'C \quad (1.1)$$

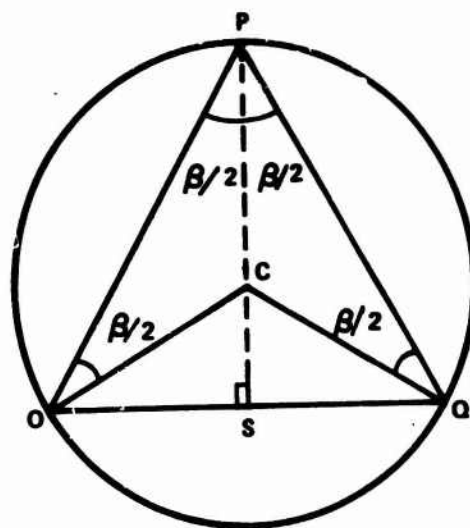


FIG. 1-3a - ISOSCELES TRIANGLE OPQ FROM FIG. 1-2

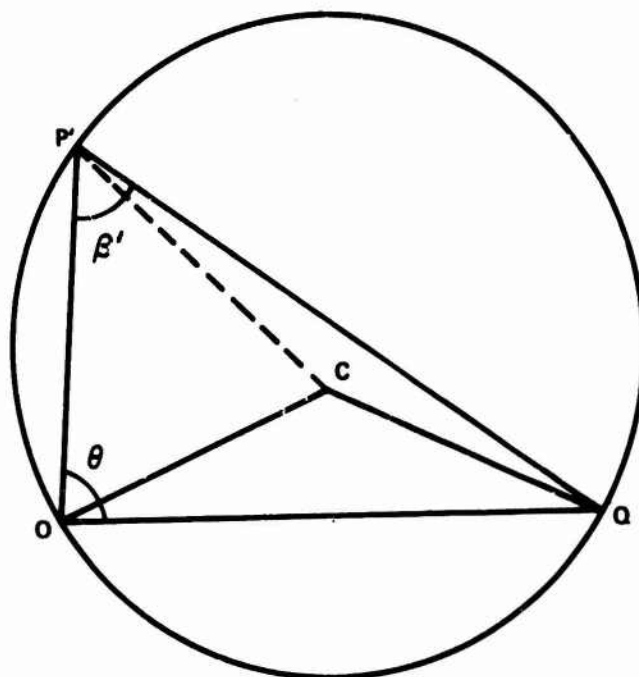


FIG. 1-3b - TRIANGLE OPQ FROM FIG. 1-2

Also, $\angle OQP' = \pi - \theta - \beta'$. But $\angle CQO = \angle COQ$, so that

$$\angle CQP' = \angle OQP' - \angle CQO = \frac{\pi}{2} - \theta - \beta' + \beta = \angle CP'Q \quad (1.2)$$

By definition,

$$\beta' = \angle OP'C + \angle CP'Q \quad (1.3)$$

Substituting eqs. 1.1 and 1.2 into eq. 1.3,

$$\beta' = \theta + \beta - \frac{\pi}{2} + \frac{\pi}{2} - \theta - \beta' + \beta$$

or $\beta' = \beta$

This result can be established in the same manner for all other points P in the same segment of the circle.

The important implication of the preceding developments is that, for any set of fixed points O and Q, a particular value of β defines a unique segment of a circle whose arc is a contour of constant β . Therefore, if the points O and Q are fixed, charted objects, the angle β observed from any position P defines a circular line of position (LOP) which passes through P. Further, if two or more such angles are measured from the same position P using different objects O and Q, the intersection point of the arcs of the circle segments circumscribing $\triangle OPQ$, $\triangle O'PQ'$, $\triangle O''PQ''$, etc., will fix the position of P within the limits of accuracy of the system. This is the theoretical basis for position fixing using the method of horizontal sextant angles.

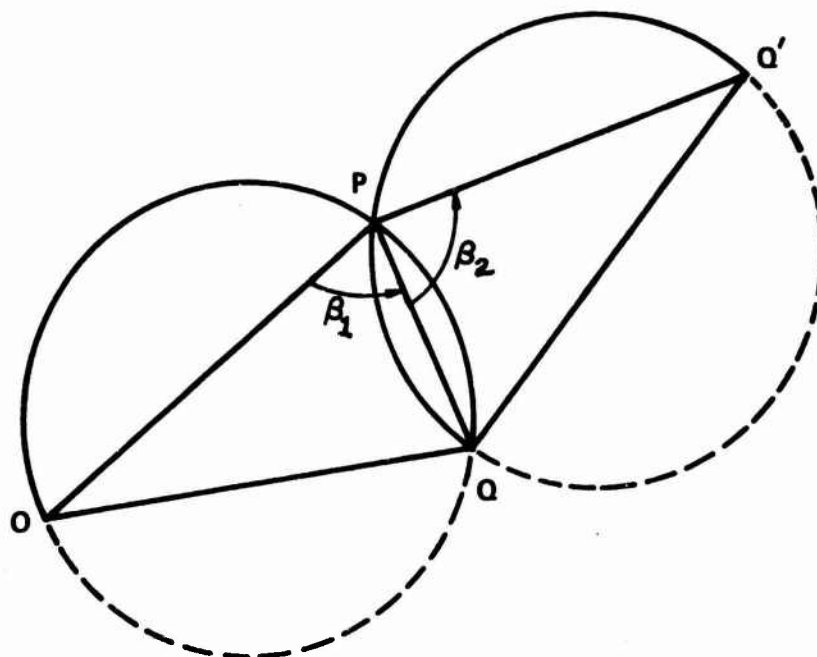
1.2 Practical Application

The method of horizontal sextant angles is used as the primary buoy anchor positioning method aboard most U. S. Coast Guard buoy tenders.

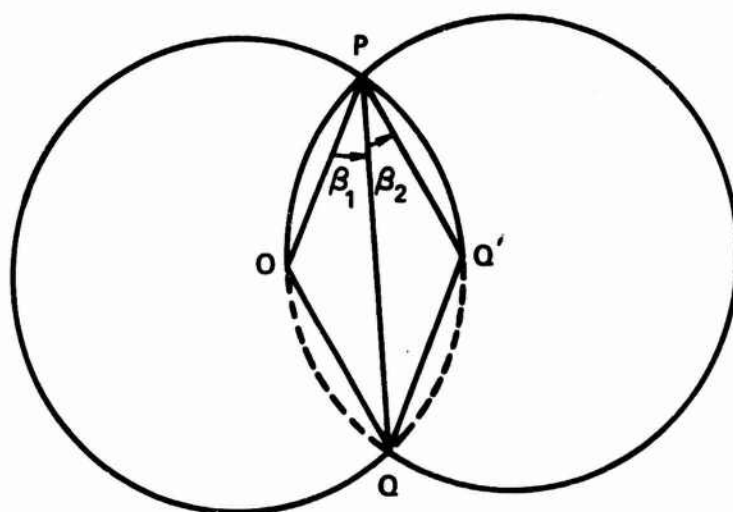
In this application, the position fix is obtained from two LOP's derived from three fixed objects. (The reliability of the fix often is assessed by comparison with a gyro bearing fix.) The case for the three-object, two-LOP fix versus fixes from other possible combinations of objects and LOP's will not be argued in this report in order to preserve the continuity of the discussion. To align the discussion with the common practice for positioning buoy anchors, only the three-object, two-LOP fix will be considered hereafter. The two general geometric situations which may result when two LOP's are obtained from three objects are shown in figs 1-4.

The example of utilizing the method of horizontal sextant angles which will be described is called the preset angle method. (The choice of this particular method for the example does not degrade the generality of subsequent developments.) The mechanics of applying this method to the buoy anchor positioning problem begins sometime before the actual operation. Files and notes of previous positioning operations for the same buoy anchor are researched to determine the three fixed objects (O, Q and Q') which are best situated for the particular intended anchor position P. Generally, alternate sets of objects are selected, if available, to permit some flexibility if the primary objects are found to be unsuitable at the time of the positioning operation. Considerations in selecting fixed objects include:

- a. visibility from the intended buoy anchor position,
- b. definition of vertical centerline, i.e., a spire is more desirable than a tangent to a point of land,



a. O, P, AND Q DEFINE LEFT LOP; Q, P, AND Q' DEFINE RIGHT LOP.



b. O, P, AND Q DEFINE RIGHT LOP; Q, P, AND Q' DEFINE LEFT LOP.

FIG. 1-4 GEOMETRIC SITUATIONS RESULTING FROM TWO-LOP HORIZONTAL SEXTANT ANGLE FIXES

- c. suitability of the angle of intersection (crossing angle) of the LOP's, and
- d. the observed angle must not exceed the maximum value which can be measured by the sextant (126° for the newest sextants).

Relatively elementary instruments are used to measure the sextant angles to be observed and the LOP crossing angle. The three-arm protractor is used to measure the angles from a standard National Ocean Survey (NOS) chart. As its name implies, this is a three-armed instrument. Its arms may be rotated about a common pivot point, and the angles between each outer arm and the center arm are read directly from a fixed scale. The vernier scale offers marked precision to one or two minutes depending upon the protractor used. There is a small hole at the pivot point which is centered over the charted buoy anchor position. Then, the arms are aligned through the charted position of each of the three fixed objects. The measured angles are recorded. In general, the largest scale chart available upon which the necessary objects are shown is used; and the angular measurements are checked by several competent personnel. The LOP crossing angle is observed usually by constructing the circular LOP's on the chart with a compass.

As the vessel proceeds to the area in which the buoy anchor will be positioned, each of the horizontal sextant angles to be observed is set on a sextant. Two competent personnel, each with one of the preset sextants, assume a prescribed position on the vessel which is selected

for its proximity to the point from which the anchor will be released and for its commanding view of the fixed objects. The vessel is maneuvered until the vertical centerlines of the objects used to obtain each LOP appear superimposed when sighting through the appropriate sextant. When this occurs, the anchor is released; and the positioning operation is complete.

1.3 Sources of System Error

The sources of error in the system as described in this chapter can be classified under three general headings. These are plotting error, primary instrument error and supplementary error. The specific components of each general heading are the errors which must be considered for the analysis of the positioning accuracy of the system.

These include the following:

(1) Plotting error

- (a) charting error of the positions of objects
- (b) instrument error in angular measurement with the three-arm protractor
- (c) human error in angular measurement with the three-arm protractor

(2) Primary instrument error

- (d) instrument error in angular measurement with the sextant
- (e) human error in angular measurement with the sextant

(3) Supplementary error

- (f) error introduced by the displacement of the

sextant angle observers from the position of
buoy anchor

- (g) error caused by the effect of current on the
anchor after it is released and/or the effect of
bottom topography on the position of the anchor
after it contacts the bottom.

The supplementary error will be neglected in the error analysis, since
its components are not truly random.

First consider the combined effect of (a) and (c). This combined
error is the source of dependent error between the two angles due to the
use of the three-arm protractor. Fig 1-5 shows a typical set of fixed
objects O, Q and Q' which are to be used to determine the position P.
Line segments PO, PQ and PQ' represent the arms of the three-arm protractor
used to measure the sextant angles to be observed. β_1 and β_2 are
the exact angular measurements of $\angle OPQ$ and $\angle QPQ'$ respectively. The
error in positioning the pivot point of the protractor directly over P
as it affects the angular measurements β_1 and β_2 is designated ϵ_{p_1}
and ϵ_{p_2} . Failure to position the arms through the exact positions
O, Q and Q' creates the errors ϵ_o , ϵ_q and $\epsilon_{q'}$ in the magnitude of
the angle measured from a reference direction (REF) to arms PO, PQ and
PQ'. The angle from REF to each arm, indicated in fig 1-5, can be sub-
tracted to give $\angle OPQ$ and $\angle QPQ'$, which define LOP-1 and LOP-2 respec-
tively, as

$$\angle OPQ = \angle (\text{REF-to-PO}) + \epsilon_o - \angle (\text{REF-to-PQ}) - \epsilon_q + \epsilon_{p_1} \quad (1.4)$$

$$\text{and } \angle QPQ' = \angle (\text{REF-to-PQ}) + \epsilon_q - \angle (\text{REF-to-PQ'}) - \epsilon_{q'} + \epsilon_{p_2}$$

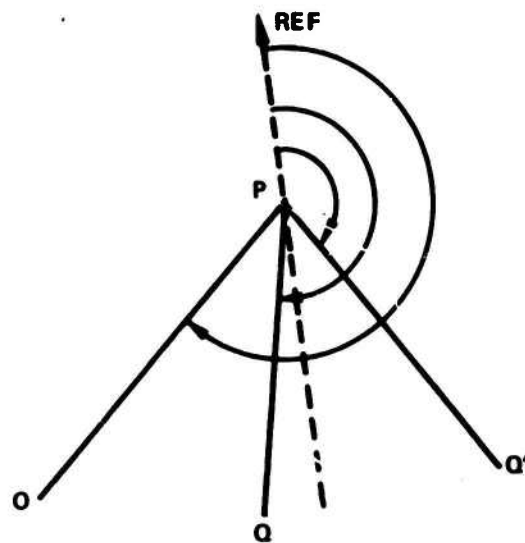


FIG. 1-5 HORIZONTAL SEXTANT ANGLE DESCRIPTION

The signs of the errors may be either positive or negative. Positive errors ϵ_o , ϵ_q and $\epsilon_{q'}$ tend to increase the magnitude of the angle between REF and the particular arm while positive errors ϵ_{p_1} and ϵ_{p_2} increase the total angle. The dependence of the error terms, shown for both angles in eqs. 1.4, upon each other is apparent from the appearance of the ϵ_q and ϵ_p terms in both equations.

The primary instrument error and (b), the three-arm protractor instrument error, are individually independent of all other errors. Their combined effect on β_1 and β_2 is designated ϵ_r and ϵ_s respectively. Adding these errors and noting that

$$\beta_1 = \angle(\text{REF-to-PO}) - \angle(\text{REF-to-PQ})$$

$$\text{and } \beta_2 = \angle(\text{REF-to-PQ}) - \angle(\text{REF-to-PQ'}),$$

eqs 1.4 become

$$\angle OPQ = \beta_1 + \epsilon_o - \epsilon_q + \epsilon_{p_1} + \epsilon_r \quad (1.5)$$

$$\text{and } \angle QPQ' = \beta_2 + \epsilon_q - \epsilon_{q'} + \epsilon_{p_2} + \epsilon_s$$

The eqs. 1.5 are the expressions for the effective horizontal sextant angles used for the positioning operation described in Section 1.2. The remainder of this presentation is dedicated to the determination of positioning accuracy from the expected angular errors ϵ .

2. POSITIONING ACCURACY

2.1 Preliminary Considerations

The ultimate goal of this report is to develop a method for determining the accuracy of a position fix obtained by horizontal sextant angles. The basic method is derived and presented in section 2.3. The assumptions which are made to permit a reasonable mathematical development of accuracy probability are the following:

- a. the combined system random error is normally distributed;
- b. any bias error has been removed from the system so that the mean of the random error is zero;

and, in the neighborhood of the observers' position P,

- c. the LOP's are coplanar;
- d. the exact and error LOP's approximate straight lines and the angular errors ϵ can be transformed into distance errors measured along a straight line which is perpendicular to the exact LOP and the error LOP; and
- e. the error LOP's are parallel to the exact LOP's.

The statistical descriptions of the individual angular errors are derived from analyses of suitable samples of random error data. (The determination of the angular error distributions of those errors which result from the use of the three-arm protractor, ϵ_o , ϵ_q , $\epsilon_{q'}$, ϵ_{p_1} and ϵ_{p_2} , from measurable distance errors in placing the arms and the pivot point is discussed in Appendix A.) Generally speaking, random physical phenomena approximate normal distributions. Further, the sum of random variables with the same distributions which are other than normal

usually will approach a normal distribution. Consequently, the assumption "a" of a normally distributed random error for the horizontal sextant angle problem is considered acceptable. The distribution of some random error variables is offset from a zero mean value by a constant value called the bias error. In order to concentrate the discussion on the analysis of the system random error, it is assumed by "b" that the bias error has been removed from the system.

The geometric model used for this analysis is shown in fig. 2-1. This model is identical to that used by Burt et al in ref. 2. The figure depicts an enlarged view of a small area in the neighborhood of the observers' position P. The effect of a one standard deviation (one - σ) error in each LOP is shown.

The combination of the one - σ error LOP's for the assumed normally distributed random error defines the elliptical probability density contour of a bivariate normal distribution. The ellipse shown in fig. 2-1 might represent the 75% probability density contour, i.e., there is a 75% probability (three chances in four) that any particular position fix will be within its boundaries. Assumptions "c", "d" and "e" are necessary for the use of this model.

The coplanarity of the LOP's, assumption "c", is considered acceptable if the fixed objects are clearly visible from the observers position and if the fixed objects and the observers position are at the same altitude. The first requirement is implicit for the application of the method of horizontal sextant angles. The latter is usually reasonable for buoy anchor positioning problems. The linearity of the LOP's and the distance error lines assumed by "d" is made temporarily to preserve

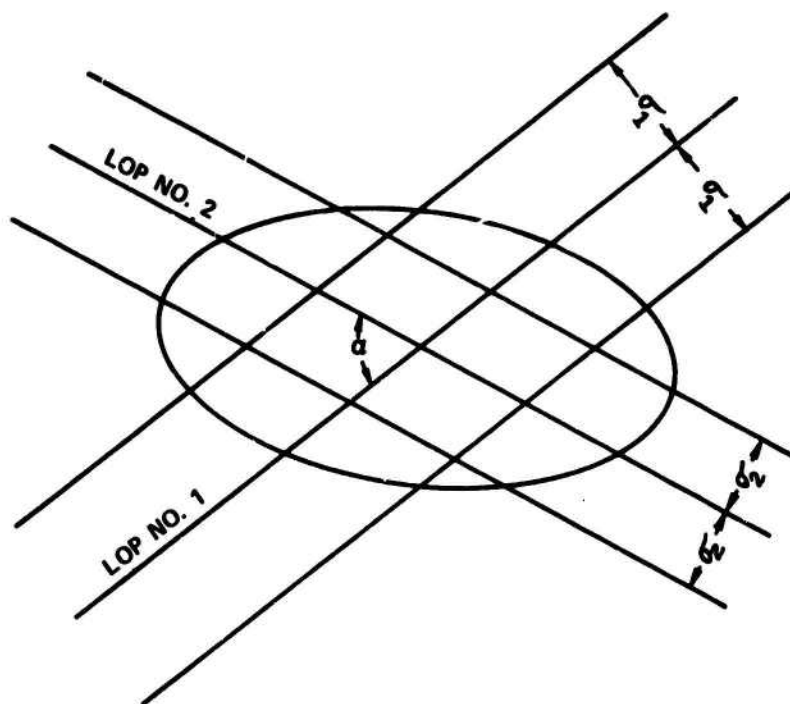


FIG. 2-1 EXPANDED VIEW OF INTERSECTION OF TWO LINES OF POSITION

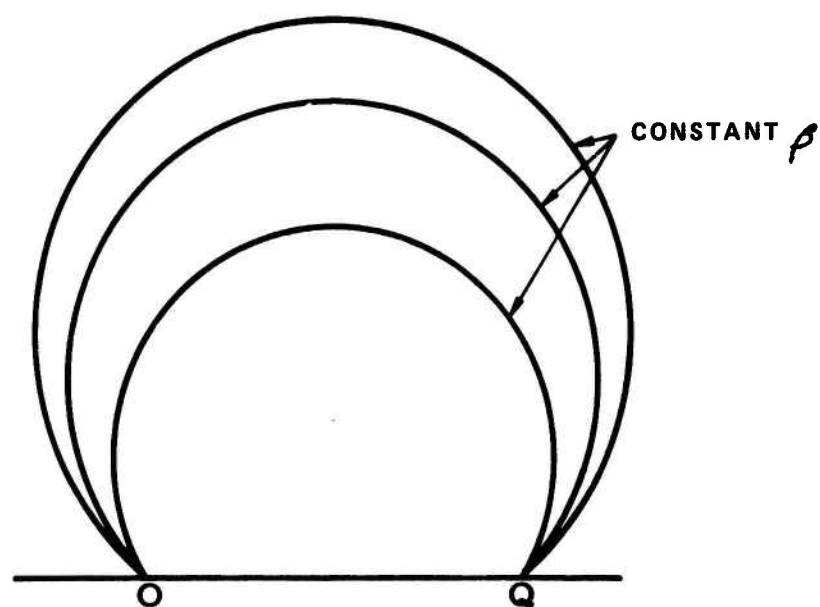


FIG. 2-2 CONTOURS OF CONSTANT β (circular LOPs)

the continuity of the discussion. Proof of the acceptability of this assumption is presented in Appendix B. Some of the developments of Chapter 3 are used in the proof. Fig. 2-2 shows that the assumption "e" of parallel exact and error LOP's is relatively poor near the points O and Q. For the relatively small expected LOP error, the LOP's will be essentially parallel everywhere except in small areas in the neighborhoods of O and Q. Consequently, this assumption, with its recognized shortcomings near the fixed objects, is considered acceptable for the purposes of this analysis.

2.2 The Probability Theory

The probability density function for a normally distributed random error variable ϵ with a zero mean value is given by

$$p(\epsilon) = \frac{1}{\sqrt{2\pi}\sigma} e^{-\frac{1}{2} \frac{\epsilon^2}{\sigma^2}} \quad (2.1)$$

where σ is the standard deviation of the distribution and σ^2 is the variance of the distribution.

The probability that a particular value of ϵ is within the limits ϵ_a and ϵ_b is determined by integrating eq. 2.1 from ϵ_a to ϵ_b . In equation form,

$$P(\epsilon_a \leq \epsilon \leq \epsilon_b) = \int_{\epsilon_a}^{\epsilon_b} p(\epsilon) d\epsilon \quad (2.2)$$

Tabular data is available for the evaluation of eq. 2.2 for any particular values of ϵ_a , ϵ_b and σ .

The general form of the joint probability density function of two normally distributed random error variables ϵ_1 and ϵ_2 , both with zero mean values, is the bivariate normal

$$p(\epsilon_1, \epsilon_2) = \frac{1}{2\pi\sigma_1\sigma_2\sqrt{1-\rho^2}} e^{-\frac{1}{2(1-\rho^2)}\left(\frac{\epsilon_1^2}{\sigma_1^2} - \frac{2\rho\epsilon_1\epsilon_2}{\sigma_1\sigma_2} + \frac{\epsilon_2^2}{\sigma_2^2}\right)} \quad (2.3)$$

where ρ is the correlation coefficient (a measure of the dependence) of ϵ_1 upon ϵ_2 .

The probability that a particular value of the combined error is within certain prescribed limits of ϵ_1 and ϵ_2 can be determined by the double integration of eq. 2.3 between these limits, i.e.,

$$P_{\epsilon} \left(\begin{matrix} \epsilon_{1a} \leq \epsilon_1 \leq \epsilon_{1b} \\ \epsilon_{2a} \leq \epsilon_2 \leq \epsilon_{2b} \end{matrix} \right) = \int_{\epsilon_{1a}}^{\epsilon_{1b}} \int_{\epsilon_{2a}}^{\epsilon_{2b}} p(\epsilon_1, \epsilon_2) d\epsilon_2 d\epsilon_1 \quad (2.4)$$

The presentation of general tabular data for the evaluation of eq. 2.4 is not feasible due to the variability of ρ from case to case. However, tabular data is available for the special case when ϵ_1 and ϵ_2 are independent ($\rho = 0$). For this special case, eq. 2.3 reduces to

$$p(\epsilon_1, \epsilon_2) = \frac{1}{2\pi\sigma_1\sigma_2} e^{-\frac{1}{2}\left(\frac{\epsilon_1^2}{\sigma_1^2} + \frac{\epsilon_2^2}{\sigma_2^2}\right)} \quad (2.5)$$

The dependent nature of each total LOP error upon the other for the three-object, two-LOP method of horizontal sextant angles was discussed in section 1.3. This dependence requires the more complicated probability density function of eq. 2.3. Fraser (ref. 3) gives a method by which the dependent errors ϵ_1 and ϵ_2 can be transformed into orthogonal, independent errors, x and y , whose probability density function is in the form of eq. 2.5. Fig. 2-3 (fig. 12 of ref. 2) can be entered, then, directly with a prescribed function of σ_x and σ_y to obtain the radius of an equivalent circular probability contour for various accuracy probabilities. (The elliptical probability density contours of the bivariate normal are converted to circular contours in order to quantify more descriptively the accuracy to be expected for a particular probability. The actual dimensions of the error ellipse are of interest only when a specific situation requires the determination of along-track and/or cross-track error.)

A suitable modification of Fraser's method for application to horizontal sextant angles and the subsequent use of fig. 2-3 will be combined to form a method by which the positioning accuracy of the system can be determined. The first task is to define the variances (σ^2) of the individual LOP error and the correlation coefficient (ρ) of the combined LOP error.

2.3 The Basic Method

The analysis begins with the definition of the equations for each LOP from eqs. 1.5 as

$$\text{LOP} - 1 = \angle \text{OPQ} = \beta_1 + \epsilon_o - \epsilon_q + \epsilon_{p_1} + \epsilon_r \quad (2.6)$$

$$\text{and } \text{LOP} - 2 = \angle \text{QPQ}' = \beta_2 + \epsilon_q - \epsilon_{q'} + \epsilon_{p_2} + \epsilon_s$$

As discussed in Section 1.3, the error components combined as ϵ_r and ϵ_s are individually independent of all other errors. Further, the errors in positioning the outer arms of the three-arm protractor, ϵ_o and $\epsilon_{q'}$, independently affect LOP - 1 and LOP - 2 respectively. These independent errors are combined to facilitate the mathematical manipulations as

$$\epsilon_i = \epsilon_o + \epsilon_r$$

$$\text{and } \epsilon_h = -\epsilon_{q'} + \epsilon_s$$

Now, the expressions for the total error affecting each LOP can be written as

$$\epsilon_1 = \epsilon_{\text{LOP} - 1} = \epsilon_i - \epsilon_q + \epsilon_{p_1} \quad (2.7a)$$

$$\text{and } \epsilon_2 = \epsilon_{\text{LOP} - 2} = \epsilon_h + \epsilon_q + \epsilon_{p_2} \quad (2.7b)$$

By definition, the variance of ϵ is equal to the expected value of the square of ϵ . In equation form

$$\sigma^2 = E[\epsilon^2] \quad (2.8)$$

Applying eq. 2.8 to eq. 2.7a,

$$\sigma_1^2 = E[(\epsilon_i - \epsilon_q + \epsilon_{p_1})^2]$$

or

$$\sigma_1^2 = E \left[\epsilon_i^2 - \epsilon_i \epsilon_q + \epsilon_i \epsilon_{p_1} - \epsilon_i \epsilon_q + \epsilon_q^2 - \epsilon_q \epsilon_{p_1} + \epsilon_i \epsilon_{p_1} - \epsilon_q \epsilon_{p_1} + \epsilon_{p_1}^2 \right] \quad (2.9)$$

Since $E[X + Y + Z + \dots] = E[X] + E[Y] + E[Z + \dots]$, eq. 2.8 can be applied to eq. 2.9 to yield

$$\sigma_1^2 = \sigma_i^2 + \sigma_q^2 + \sigma_{p_1}^2 - 2 E \left[\epsilon_i \epsilon_q + \epsilon_q \epsilon_{p_1} - \epsilon_i \epsilon_{p_1} \right] \quad (2.10)$$

The last three terms in eq. 2.10 are the covariance (μ) terms which express the dependence of the random variables. However, as stated previously, the

ϵ_i error is individually independent of all other errors, so that

$\mu_{iq} = E[\epsilon_i \epsilon_q] = 0$ and $\mu_{ip_1} = E[\epsilon_i \epsilon_{p_1}] = 0$. Also, assuming that the error in aligning arm PQ directly through Q is independent of that in positioning the pivot point directly over point P, $\mu_{qp_1} = E[\epsilon_q \epsilon_{p_1}] = 0$;

and all the covariance terms vanish. Eq. 2.10 becomes

$$\sigma_1^2 = \sigma_i^2 + \sigma_q^2 + \sigma_{p_1}^2 \quad (2.11)$$

A similar sequence of operations on eq. 2.7b yields

$$\sigma_2^2 = \sigma_h^2 + \sigma_q^2 + \sigma_{p_2}^2 \quad (2.12)$$

The correlation coefficient ρ of ϵ_1 and ϵ_2 is defined as

$$\rho = \frac{\mu_{12}}{\sigma_1 \sigma_2} \quad (2.13)$$

where $\mu_{12} = E[\epsilon_1 \epsilon_2]$ is the covariance of ϵ_1 and ϵ_2 . (2.14)

Substituting eqs. 2.7 into the expression for the covariance, eq. 2.14,

$$\mu_{12} = E[(\epsilon_i - \epsilon_q + \epsilon_{p_1})(\epsilon_h + \epsilon_q + \epsilon_{p_2})]$$

or

$$\begin{aligned} \mu_{12} = E[& \epsilon_i \epsilon_h + \epsilon_i \epsilon_q + \epsilon_i \epsilon_{p_2} - \epsilon_q \epsilon_h - \epsilon_q^2 - \epsilon_q \epsilon_{p_2} \\ & + \epsilon_{p_1} \epsilon_h + \epsilon_{p_1} \epsilon_q + \epsilon_{p_1} \epsilon_{p_2}] \end{aligned} \quad (2.15)$$

Since ϵ_i and ϵ_h are independent in themselves and ϵ_q is independent of ϵ_p , eq. 2.15 reduces to

$$\mu_{12} = E[\epsilon_{p_1} \epsilon_{p_2}] - \sigma_q^2 \quad (2.16)$$

The components of ϵ_{p_1} and ϵ_{p_2} are derived in Appendix A as

$$\epsilon_{p_1} = - \Delta \theta_1 + \Delta \theta_2 \quad (A.12)$$

$$\text{and } \epsilon_{p_2} = - \Delta \theta_2 - \Delta \kappa_2 \quad (A.8)$$

where $\Delta \theta_1$, $\Delta \theta_2$ and $\Delta \kappa_2$ are angular changes defined in Appendix A (figs. A-3 and A-4).

Therefore,

$$E[\epsilon_{p_1} \epsilon_{p_2}] = E[(- \Delta \theta_1 + \Delta \theta_2)(- \Delta \theta_2 - \Delta \kappa_2)]$$

$$\text{or } E \left[\epsilon_{p_1} \epsilon_{p_2} \right] = E \left[\Delta \theta_1 \Delta \theta_2 + \Delta \theta_1 \Delta \kappa_2 - \Delta \theta_2^2 - \Delta \theta_2 \Delta \kappa_2 \right] \quad (2.17)$$

The individual angular changes, $\Delta \theta_1$, $\Delta \theta_2$ and $\Delta \kappa_2$, are individually independent of any other single angular change so that eq. 2.17 may be written as

$$E \left[\epsilon_{p_1} \epsilon_{p_2} \right] = E \left[- \Delta \theta_2^2 \right] = - \sigma_{\Delta \theta_2}^2 \quad (2.18)$$

$$\text{and } \mu_{12} = - \sigma_{\Delta \theta_2}^2 - \sigma_q^2 \quad (2.19)$$

Now, substituting eqs. 2.11, 2.12 and 2.19 into eq. 2.13,

$$\rho = \frac{-(\sigma_{\Delta \theta_2}^2 + \sigma_q^2)}{(\sqrt{\sigma_i^2 + \sigma_q^2 + \sigma_{p_1}^2})(\sqrt{\sigma_h^2 + \sigma_q^2 + \sigma_{p_2}^2})} \quad (2.20)$$

Eqs. 2.11, 2.12 and 2.20 define all of the parameters required in eq. 2.3.

In order to continue the development into Fraser's method for eliminating the dependence of the LOP errors, it is necessary to convert the parameters of eq. 2.3 as defined by eqs. 2.11, 2.12 and 2.19 into distance units measured over a straight line which is perpendicular to the exact and the error LOP's. Ultimately, this conversion is necessary to obtain the radius of a particular circular probability density contour, which must be in distance units. Assume that there is a factor \hat{K} which meets the stated conversion requirements. This is expressed in equation form as

$$\epsilon_d = \hat{K} \epsilon_a \quad (2.21)$$

where ϵ_d is the error in distance units

and ϵ_a is the error in angular units.

Applying eq. 2.21 to ϵ_1 gives $\epsilon_{1d} = \hat{k}_1 \epsilon_1$. This implies that

$$\sigma_{1d}^2 = E \left[(\hat{k}_1 \epsilon_1)^2 \right] \quad (2.22)$$

$$\text{But, } E \left[(\hat{k}_1 \epsilon_1)^2 \right] = \hat{k}_1^2 E \left[\epsilon_1^2 \right]$$

$$\text{so that } \sigma_{1d}^2 = \hat{k}_1^2 E \left[\epsilon_1^2 \right] \quad (2.23)$$

$$\text{Similarly, } \sigma_{2d}^2 = \hat{k}_2^2 E \left[\epsilon_2^2 \right] \quad (2.24)$$

Using eq. 2.8 and substituting eq. 2.11 or eq. 2.12 as appropriate, eqs.

2.23 and 2.24 become

$$\sigma_{1d}^2 = \hat{k}_1^2 (\sigma_i^2 + \sigma_q^2 + \sigma_{p_1}^2) \quad (2.25)$$

$$\text{and } \sigma_{2d}^2 = \hat{k}_2^2 (\sigma_h^2 + \sigma_q^2 + \sigma_{p_2}^2) \quad (2.26)$$

The same procedure can be used to convert the angular covariance term into distance units. Using eqs. 2.14 and 2.21,

$$\mu_{12d} = E \left[(\hat{k}_1 \epsilon_1)(\hat{k}_2 \epsilon_2) \right] = \hat{k}_1 \hat{k}_2 E \left[\epsilon_1 \epsilon_2 \right] \quad (2.27)$$

or, substituting eq. 2.19 into eq. 2.27,

$$\mu_{12d} = - \hat{k}_1 \hat{k}_2 (\sigma_{\theta_2}^2 + \sigma_q^2) \quad (2.28)$$

Note that when the variances and covariance in distance units given by eqs. 2.25, 2.26 and 2.28 are substituted into the general expression for

the correlation coefficient ρ (eq. 2.13), the \hat{K} factors cancel so that

$$\rho = \frac{\mu_{12}}{\sigma_1 \sigma_2} = \frac{\mu_{12d}}{\sigma_{1d} \sigma_{2d}} \quad (2.29)$$

The correlation coefficient ρ is unaffected by the conversion to distance units and is still given by eq. 2.20. Chapter 3 is dedicated to the derivation and analysis of the conversion factor \hat{K} .

The variance and covariance terms in distance units, as defined by eqs. 2.25, 2.26 and 2.28, permit the application of Fraser's method directly. (Fraser's method is abstracted herein for the purposes of this discussion. The details of the entire development are given in ref. 3.) Since the LOP crossing angle (α in fig. 2-1) is not necessarily 90° , the first step is to transform the error variables onto orthogonal axes. The transformation is given as

$$\epsilon_{1d} = E_1 \quad (2.30)$$

$$\text{and } \epsilon_{2d} = \frac{E_1 - E_2 \tan \alpha}{\sec \alpha}$$

where E_1 and E_2 are the error variables along the new orthogonal axes and α is the LOP crossing angle.

The transformation of eqs. 2.30 can be used to obtain the joint probability density function of E_1 , E_2 as

$$P(E_1, E_2) = \frac{1}{2\pi\sigma_{E_1}\sigma_{E_2}\sqrt{1-\rho_1^2}} e^{-\frac{1}{2(1-\rho_1^2)}\left(\frac{E_1^2}{\sigma_{E_1}^2} - \frac{2\rho_1 E_1 E_2}{\sigma_{E_1}\sigma_{E_2}} + \frac{E_2^2}{\sigma_{E_2}^2}\right)} \quad (2.31)$$

where $\sigma_{E_1} = \sigma_{1d}$

$$\sigma_{E_2} = \frac{1}{|\tan\alpha|} \sqrt{\sigma_{1d}^2 + \sigma_{2d}^2 \sec^2\alpha - 2\mu_{12d} \sec\alpha}$$

$$U_{12} = E[E_1 E_2] = -\frac{1}{\tan\alpha} (\sigma_{1d}^2 - \mu_{12d} \sec\alpha)$$

$$\rho_1 = \frac{U_{12}}{\sigma_{E_1}\sigma_{E_2}} = \frac{\sigma_{1d}^2 - \mu_{12d} \sec\alpha}{\sigma_{1d} \sqrt{\sigma_{1d}^2 + \sigma_{2d}^2 \sec^2\alpha - 2\mu_{12d} \sec\alpha}}$$

Although the error axes are now orthogonal, the cross product term in the exponent of e in eq. 2.31 indicates the dependence of E_2 upon E_1 . In order to eliminate the cross product term, the coordinate axes are rotated by another linear change of variables. The transformation is stated as follows:

$$E_1 = x \cos\phi - y \sin\phi \quad (2.32)$$

$$E_2 = x \sin\phi + y \cos\phi$$

where ϕ is the angle through which the axes are rotated.

The derivation of ref. 3 shows that the expression for ϕ must be

$$\rho = \frac{1}{2} \tan^{-1} \left[\frac{2 \rho_1 \sigma_{E_1} \sigma_{E_2}}{\sigma_{E_1}^2 - \sigma_{E_2}^2} \right] \quad (2.33)$$

This transformation for the rotation of the coordinate axes is discussed in ref. 4 also. When eqs. 2.32 and 2.33 are substituted into eq. 2.31, the resulting probability density function is

$$P(x,y) = \frac{1}{2\pi \sigma_x \sigma_y} e^{-\frac{1}{2} \left(\frac{x^2}{\sigma_x^2} + \frac{y^2}{\sigma_y^2} \right)} \quad (2.34)$$

$$\text{where } \sigma_x = \sqrt{\sigma_{E_1}^2 \cos^2 \rho + \sigma_{E_2}^2 \sin^2 \rho + 2U_{12} \sin \rho \cos \rho} \quad (2.35)$$

$$\text{and } \sigma_y = \sqrt{\sigma_{E_1}^2 \sin^2 \rho + \sigma_{E_2}^2 \cos^2 \rho - 2U_{12} \sin \rho \cos \rho}$$

Eqs. 2.35 define the standard deviations σ_x and σ_y of the independent variables x and y . Now, fig. 2-3 can be entered with the smaller of the ratios $\frac{\sigma_x}{\sigma_y}$ or $\frac{\sigma_y}{\sigma_x}$. This value and the desired accuracy probability define a value of K . The radius of the equivalent circular probability density contour is calculated by

$$R = K \sigma_b \quad (2.36)$$

where σ_b is the larger of σ_x and σ_y .

This concludes the development of the basic method for determining the positioning accuracy of the method of horizontal sextant angles. As stated

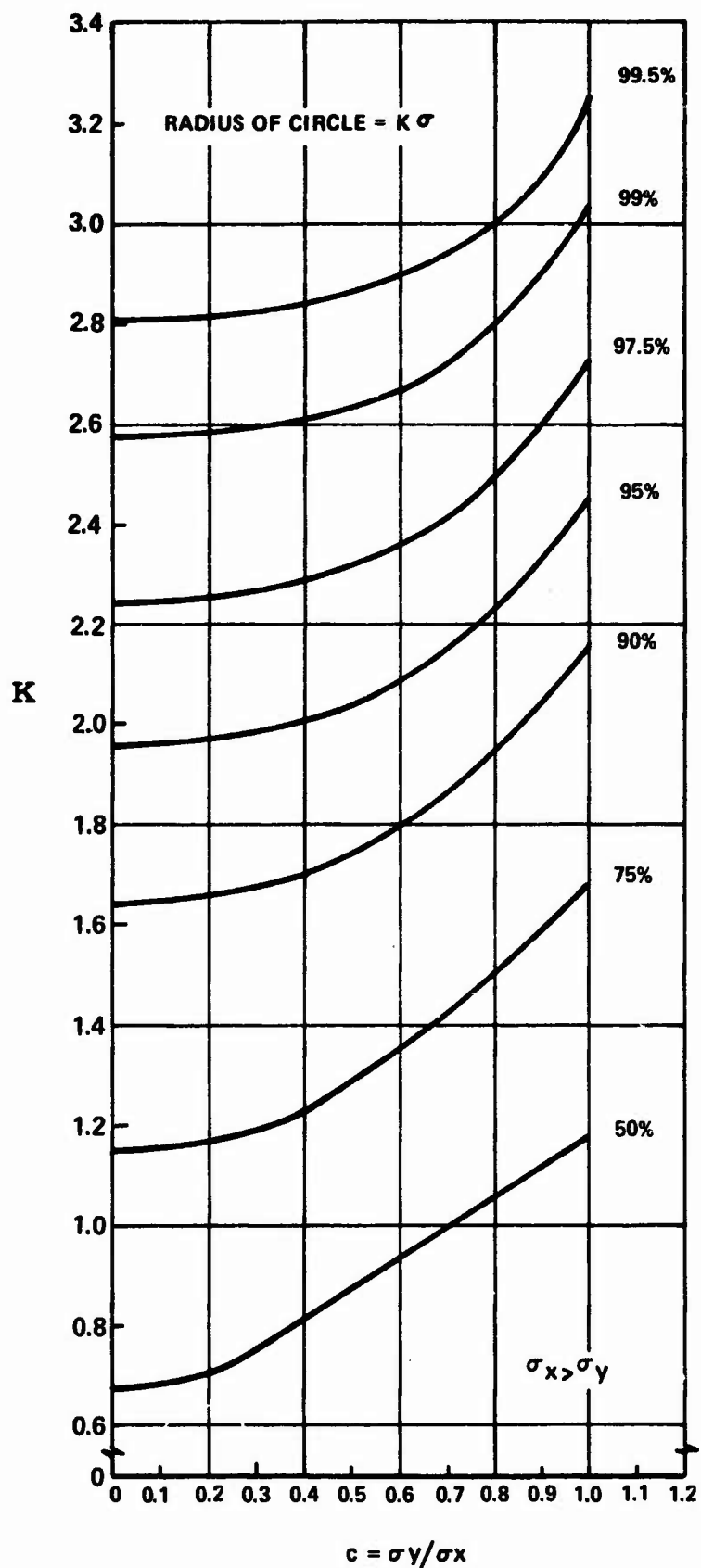


FIG. 2-3 CONVERSION OF PROBABILITY ELLIPSE TO CIRCLE

previously, the derivation and analysis of the conversion factor \hat{K} used to convert the angular error to distance error is presented in Chapter 3. The derivation of a means for calculating the LOP crossing angle α for a three-object, two-LOP position fix is included as Chapter 4. Finally, an example of a practical application of the complete method to a buoy positioning problem is given in Chapter 5. It should be noted that the presentation will continue through the example problem without the benefit of suitable, published human factors error data. The consequent assumptions made in Chapter 5 for the purposes of the example are explicit therein.

3. THE GEOMETRIC MULTIPLICATION OF PRECISION (GMOP)

3.1 The Role of the GMOP

The development of Section 2.3 presumed the existence of a conversion factor \hat{K} , defined by eq. 2.21, which can change the angular variances of the individual LOP's and the angular covariance of the combined LOP's into distance units. Further, in order to conform to the geometric model of fig. 2-1, it is necessary that, in the neighborhood of the observers' position P, the resulting distance error is measured over a straight line which is perpendicular to the exact and the error LOP's (assumption "d", Section 2.1). It is the purpose of this chapter to develop and study a suitable conversion method within the geometric constraints of the system. The ultimate goal is to find some function which is independent of the baseline length (the distance between the fixed objects, designated A) such that the product of this function, evaluated at any point P, and A will yield \hat{K} . Combining this concept with eq. 2.21, this function, named the Geometric Multiplication of Precision (GMOP), is expressed in equation form as

$$GMOP = \frac{\hat{K}}{A} = \frac{\epsilon_d}{A \epsilon_a} \quad (3.1)$$

where ϵ_d is the error in distance units,

ϵ_a is the error in angular units,

and A is the baseline length

The reader familiar with electronic triangulation systems will recognize the analogy between the GMOP and the GDOP (Geometric Dilution of Precision)

commonly used for the electronic systems. The significant difference between the two is that GMOP equals zero at the fixed objects O and Q.

At this point a brief discussion of the direction of the following development is appropriate. The direction of the development is set by the desire to describe the GMOP as a function of the magnitude of the gradient of β , $|\vec{\nabla}\beta|$. The logic of this choice is apparent when the the desired features of the GMOP are compared with the inherent traits of the gradient of β , $\vec{\nabla}\beta$. The magnitude of $\vec{\nabla}\beta$ converts distance traveled between contours of constant β (the LOP's) along the path of maximum change in β to an angular change in β .* The direction of $\vec{\nabla}\beta$ along the path of maximum change in β requires that it is perpendicular to the contours of constant β . Fig. 3-1 illustrates the relationship between the contours of constant β and curves of $\vec{\nabla}\beta$. (The circular nature of the curves of $\vec{\nabla}\beta$ as presented in fig. 3-1 is shown to be accurate during the analysis of Appendix B.) Obviously, the inverse of $|\vec{\nabla}\beta|$ meets the requirement to convert angular measure to distance units within the geometric constraints of the system. Further, the fact that $\vec{\nabla}\beta$ is perpendicular to contours of constant β indicates that the requirement to measure the error in distance units along a straight line which is perpendicular to the exact and error LOP's may be approximated by measuring the error along curves of $\vec{\nabla}\beta$. Therefore, there is a strong possibility of fulfilling all of the requirements of GMOP with a function of $|\vec{\nabla}\beta|$. The development begins with the derivation of the mathematical expression for the LOP in Section 3.2.

3.2 The Mathematical Expression for an LOP

Consider the circular LOP shown in fig. 3-2. Again, the observer's position is P and O and Q are the fixed objects used to generate the hori-

*The conversion is from distance units to radians.

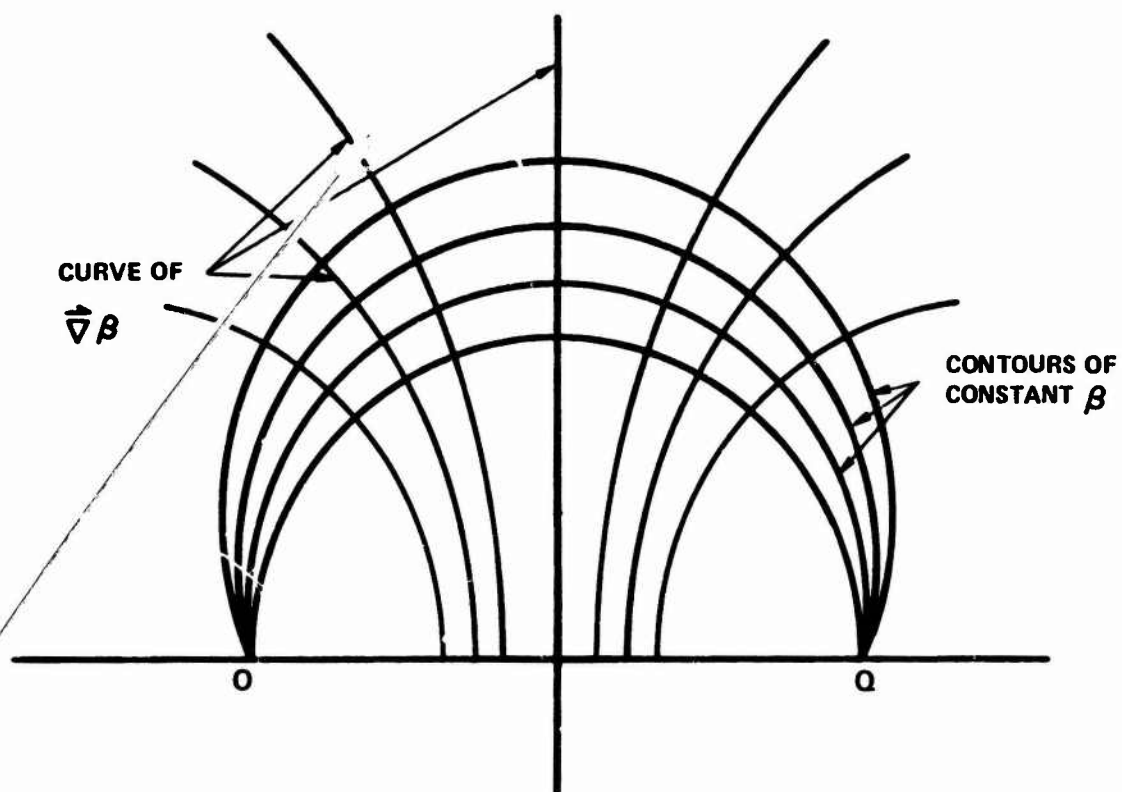


FIG. 3-1 THE RELATIONSHIP BETWEEN CONTOURS OF CONSTANT β AND $\nabla\beta$ CURVES

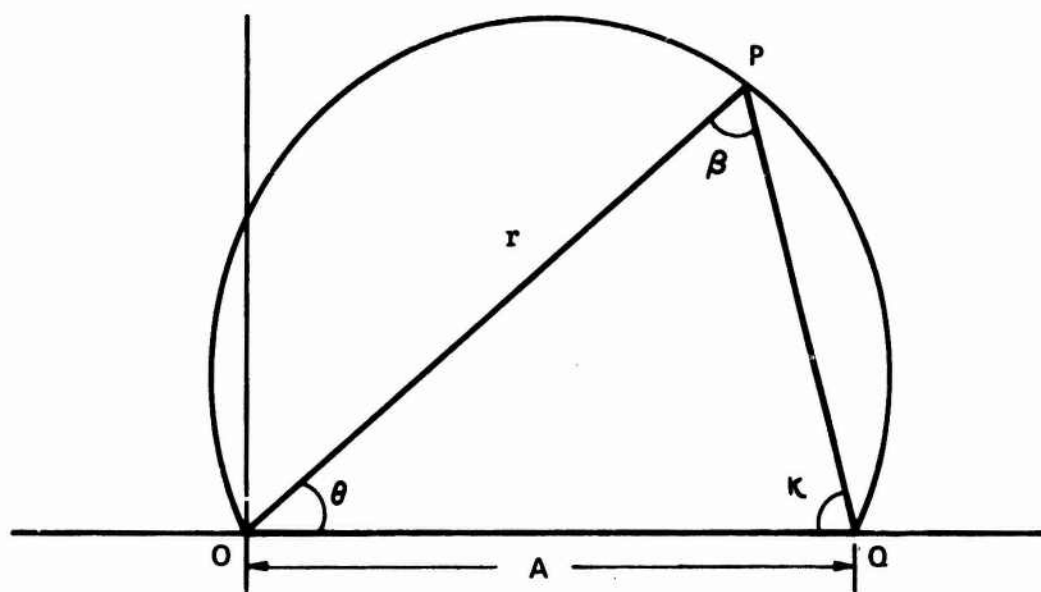


FIG. 3-2 CIRCULAR LOOP SHOWING PERTINENT PARAMETERS

zontal sextant angle. The coordinate system is chosen with point O at the origin. (It is very important to understand that this representation and the analysis which follows applies to any sextant angle generated from two fixed objects, i.e., the points O and Q are representative of any set of baseline objects.) It is expedient in this case to use the polar coordinate system where \vec{r} is the position vector of any point in the plane of the coordinate system. The position vector \vec{r} has magnitude r and a direction defined by the angle θ between \vec{r} and the baseline axis. The variables A and β have been defined as the distance between O and Q along the baseline and the exact measurement of the horizontal sextant angle respectively. Referring to fig. 3-2 and using the law of sines;

$$\frac{r}{\sin \kappa} = \frac{A}{\sin \beta} \quad (3.2)$$

Substituting for κ

$$\frac{r}{\sin [\pi - (\beta + \theta)]} = \frac{A}{\sin \beta}$$

Noting that $\sin [\pi - (\beta + \theta)] = \sin (\beta + \theta)$,

$$\frac{r}{\sin (\beta + \theta)} = \frac{A}{\sin \beta}$$

Finally, $\sin (\beta + \theta) = \sin \beta \cos \theta + \cos \beta \sin \theta$

so that

$$r = A(\cos \theta + \cot \beta \sin \theta) \quad (3.3)$$

Eq. 3.3 represents the LOP in polar coordinates in terms of r , A , θ and β .

3.3 The Derivation of the GMOP

Eq. 3.3 can be manipulated to yield an expression for β in terms of r , A and θ . The manipulation yields

$$\beta = \cot^{-1} \left[\frac{r}{A} \csc \theta - \cot \theta \right] \quad (3.4)$$

The general form of the gradient of β in polar coordinates is

$$\vec{\nabla} \beta = \frac{\partial \beta}{\partial r} \hat{r} + \frac{1}{r} \frac{\partial \beta}{\partial \theta} \hat{\theta} \quad (3.5)$$

where \hat{r} and $\hat{\theta}$ are unit vectors in the r and θ directions respectively.

The components of eq. 3.5 may be derived from eq. 3.4 as

$$\frac{\partial \beta}{\partial r} = - \frac{1}{A} \csc \theta \sin^2 \beta \quad (3.6)$$

$$\text{and } \frac{1}{r} \frac{\partial \beta}{\partial \theta} = - \frac{1}{A} \csc \theta \sin^2 \beta \left[\frac{\sin \theta - \cot \beta \cos \theta}{\cos \theta + \cot \beta \sin \theta} \right]$$

(The details of the derivation from eq. 3.4, through eq. 3.8 are presented in Appendix C. Also, an understanding of the development through eq. 3.8 should permit the reader to follow the analysis of Appendix B, the proof of the acceptability of assumption "d" of Section 2.1.)

The magnitude of $\vec{\nabla} \beta$ is given by

$$|\vec{\nabla} \beta| = \sqrt{\left(\frac{\partial \beta}{\partial r} \right)^2 + \left(\frac{1}{r} \frac{\partial \beta}{\partial \theta} \right)^2} \quad (3.7)$$

Substituting eqs. 3.6 into eq. 3.7 yields

$$|\vec{\nabla}\beta| = \frac{\csc\theta \sin\beta}{A(\cos\theta + \cot\beta \sin\theta)} \quad (3.8)$$

Now, the GMOP may be derived from eq. 3.8 in the desired form of eq. 3.1 as

$$\text{GMOP} = \frac{1}{A |\vec{\nabla}\beta|} = \sin\theta \csc\beta (\cos\theta + \cot\beta \sin\theta) \quad (3.9)$$

3.4 The Nature of the GMOP

At this point the behavior of eq. 3.9 over the entire ranges of β and θ is of interest. The equation may be put in a more suitable analytical form by first expanding as

$$\text{GMOP} = \csc\beta \sin\theta \cos\theta + \csc\beta \cot\beta \sin^2\theta \quad (3.10)$$

Substituting into eq. 3.10 the trigonometric identities

$$\sin\theta \cos\theta = \frac{1}{2} \sin 2\theta$$

$$\text{and } \sin^2\theta = \frac{1}{2} - \frac{1}{2} \cos 2\theta$$

yields

$$\text{GMOP} = \frac{1}{2} \csc\beta \sin 2\theta + \frac{1}{2} \csc\beta \cot\beta - \frac{1}{2} \csc\beta \cot\beta \cos 2\theta \quad (3.11)$$

Letting

$$C = \frac{1}{2} \csc\beta \quad \text{and} \quad D = \frac{1}{2} \csc\beta \cot\beta,$$

$$\text{GMOP} = D + C \sin 2\theta + (-D) \cos 2\theta$$

$$\text{or } \text{GMOP} = D - \sqrt{C^2 + D^2} \cos(2\theta + \gamma) \quad (3.12)$$

$$\text{where } \gamma = \tan^{-1}\left(\frac{C}{D}\right)$$

Let $E = \sqrt{C^2 + D^2}$ and notice that $\frac{C}{D} = \tan \beta$, so that

$$GMOP = D - E \cos(2\theta + \beta) \quad (3.13)$$

The nature of the GMOP is readily discernible from eq. 3.13. Particular features include the following:

- a. For any β , GMOP consists of a constant D from which some portion of a cosine function is subtracted.
- b. The sinusoidal portion of GMOP cycles once each π radians.
- c. Increasing β between 0° and 90° causes a decrease in D and E and shifts the cosine curve to the left.
- d. Noting that

$$\begin{aligned} E &= \sqrt{C^2 + D^2} = \sqrt{\frac{1}{4} \csc^2 \beta + \frac{1}{4} \csc^2 \beta \cot^2 \beta} = \frac{1}{2} \csc \beta \sqrt{1 + \cot^2 \beta} \\ &= \frac{1}{2} \csc^2 \beta, \end{aligned}$$

eq. 3.13 can be written as

$$GMOP = \frac{1}{2} \csc^2 \beta \cos \beta - \frac{1}{2} \csc^2 \beta \cos(2\theta + \beta)$$

Values of θ may vary from zero for P located at Q to $\pi - \beta$ for P at O (see fig. 3-2).

At these boundary values of θ ,

$$\theta = 0, GMOP = \frac{1}{2} \csc^2 \beta \cos \beta - \frac{1}{2} \csc^2 \beta \cos \beta = 0$$

$$\theta = \pi - \beta, \text{ GMOP} = \frac{1}{2} \csc^2 \beta \cos \beta - \frac{1}{2} \csc^2 \beta \cos(2\pi - 2\beta + \beta) = 0$$

This is the expected result since the contours of constant β (the circular LOP's) converge at 0 and Q (see fig. 2-2).

- e. The variation of θ from 0 to $\pi - \beta$ causes the truncation of the cosine curve at a distance β from $2\theta + \beta = 0$ and from $2\theta + \beta = 2\pi$; thus, all possible values of $2\theta + \beta$ yield $\cos(2\theta + \beta) \leq \cos \beta$ so that the GMOP is always positive.
- f. Intuitively, the points M_β , which lie on the perpendicular bisector of OQ in fig. 3-3, should be the points at which GMOP is maximum for any given β . As indicated in the figure, for the points M_β , $\theta = \frac{\pi - \beta}{2}$. The derived equation may be checked for agreement as follows:

$$\left. \frac{\partial \text{GMOP}}{\partial \theta} \right|_\beta = 2E \sin(2\theta + \beta) = \csc^2 \beta \sin(2\theta + \beta) = 0 \quad (3.14)$$

for the non-trivial case, eq. 3.14 implies that

$$2\theta + \beta = n\pi \quad (n = 0, 1, 2, \dots)$$

For any β in the range of interest, the only one of the values which $2\theta + \beta$ assumes is π . Consequently,

$$2\theta + \beta = \pi$$

which yields $\theta = \frac{\pi - \beta}{2}$ for maximum GMOP ($\beta = \text{const}$)

- g. Finally, the combined implications of "e" and "f" above indicate that the values of GMOP are symmetrical about the perpendicular bisector of OQ.

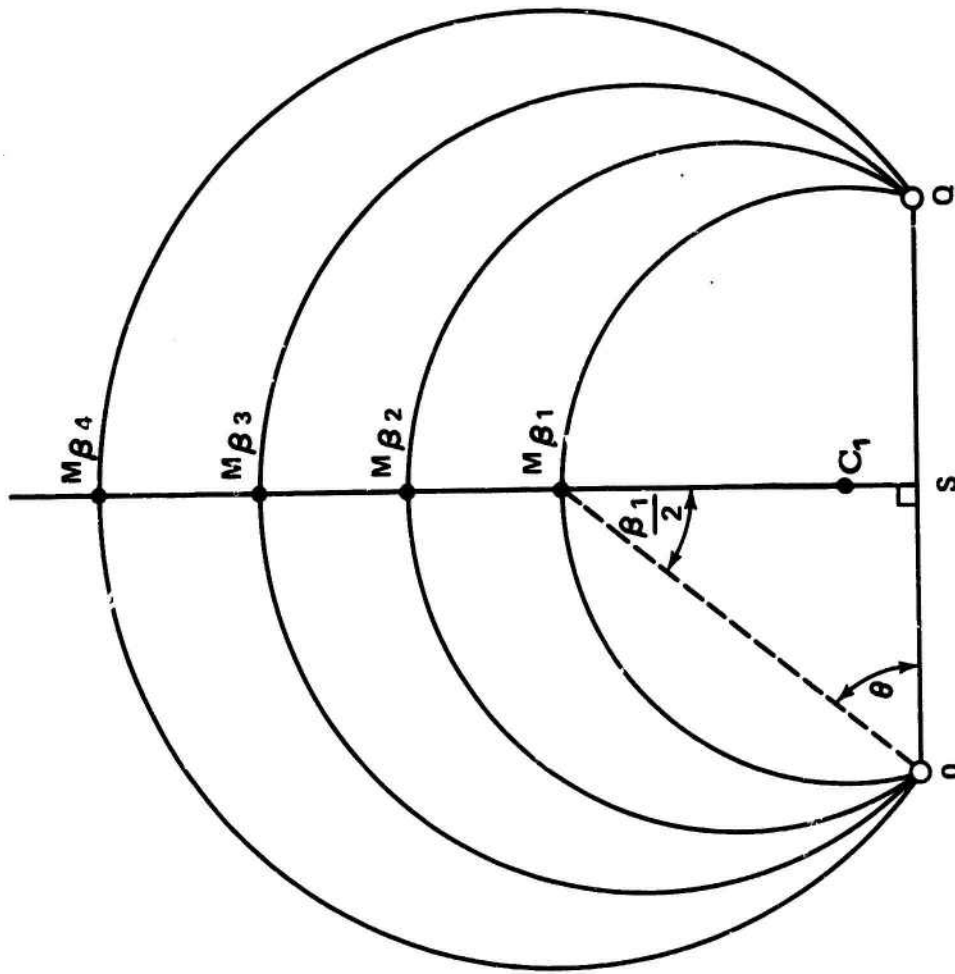


Figure 3-3. Circular LOPs showing points M_{β} of maximum GMOP.

Items "d" through "g" above indicate that the mathematical representation of the GMOP behaves as expected at several check points. It is concluded from these favorable results that eq. 3.9 does describe a function which satisfies the form requirement of eq. 3.1 and converts angular errors to distance units within the system constraints. Fig. 3-4 shows curves of GMOP vs θ for 20-degree increments of β from 5° to 125° (within the range of the newest sextants). The curves are presented to demonstrate the changing shape as β varies. Additionally, contours of constant GMOP are shown in fig. 3-5. This type of representation usually aids in the visualization of the physical situation.

3.5 The Feasibility of Linear Interpolation for GMOP

An investigation of the feasibility of linear interpolation between the curves of fig. 3-4 to obtain values of GMOP for intermediate values of β and between curves of GMOP vs β for incremental θ in order to obtain GMOP for intermediate values of θ is of interest. For the first case, values of GMOP (θ_1, β_1) and GMOP (θ_1, β_3) would be obtained from fig. 3-4. Then, the linear interpolation could be performed to obtain GMOP (θ_1, β_2). The second case implies that GMOP (θ_1, β_1) and GMOP (θ_3, β_1) could be used to find GMOP (θ_2, β_1) by linear interpolation. The combination of these two possibilities would yield a relatively concise table from which GMOP could be determined for any possible β and θ . The advantages of such a presentation are obvious. For exact linear interpolation in the first case, $\left. \frac{\partial \text{GMOP}}{\partial \beta} \right|_{\theta}$ must be constant, i.e., there must be a linear relationship between β and GMOP for any constant θ . Likewise, exact linear

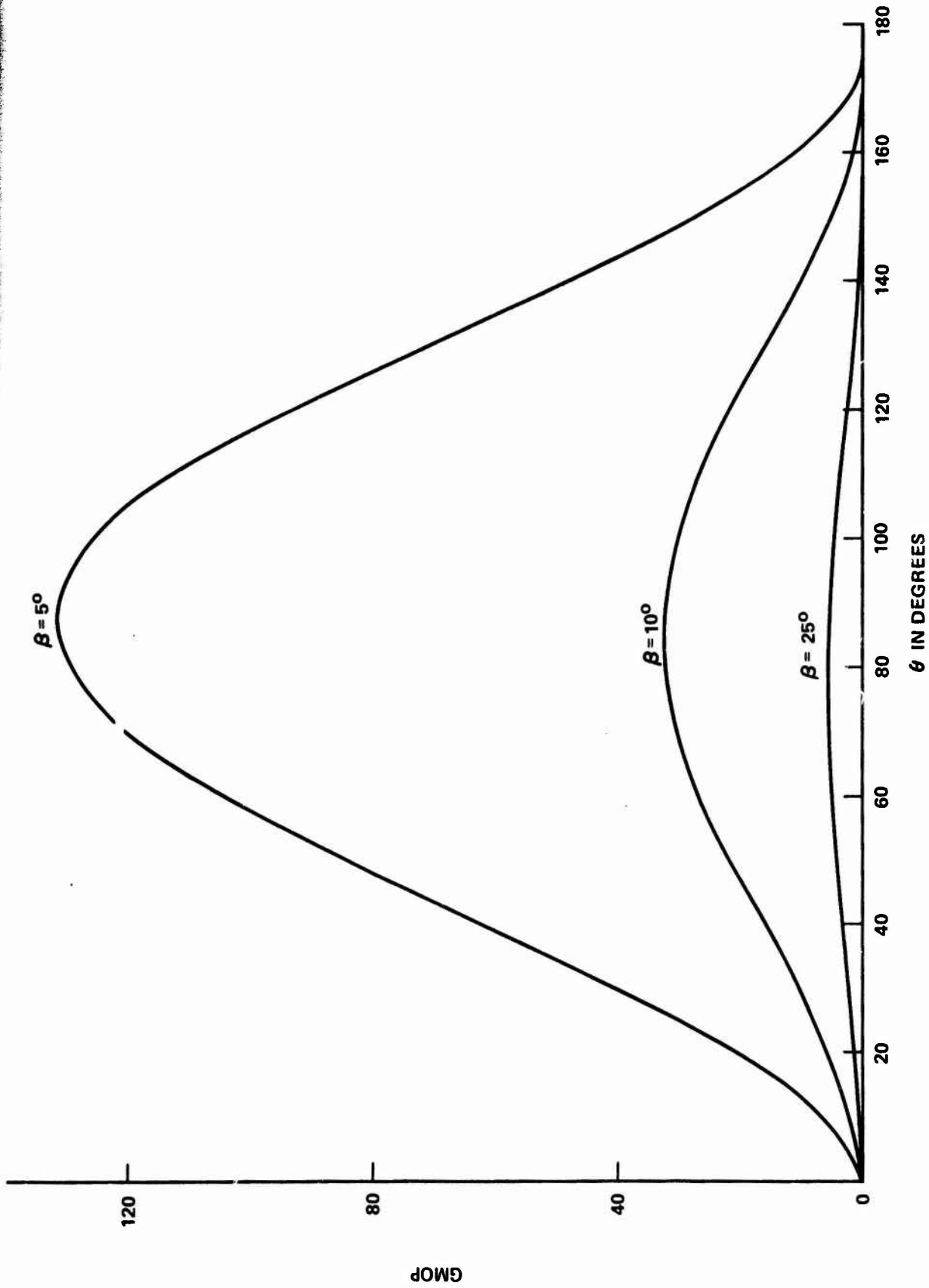


Figure 3-4a. Curves of GMOP vs θ , for $\beta = 5^\circ, 10^\circ, 25^\circ$.

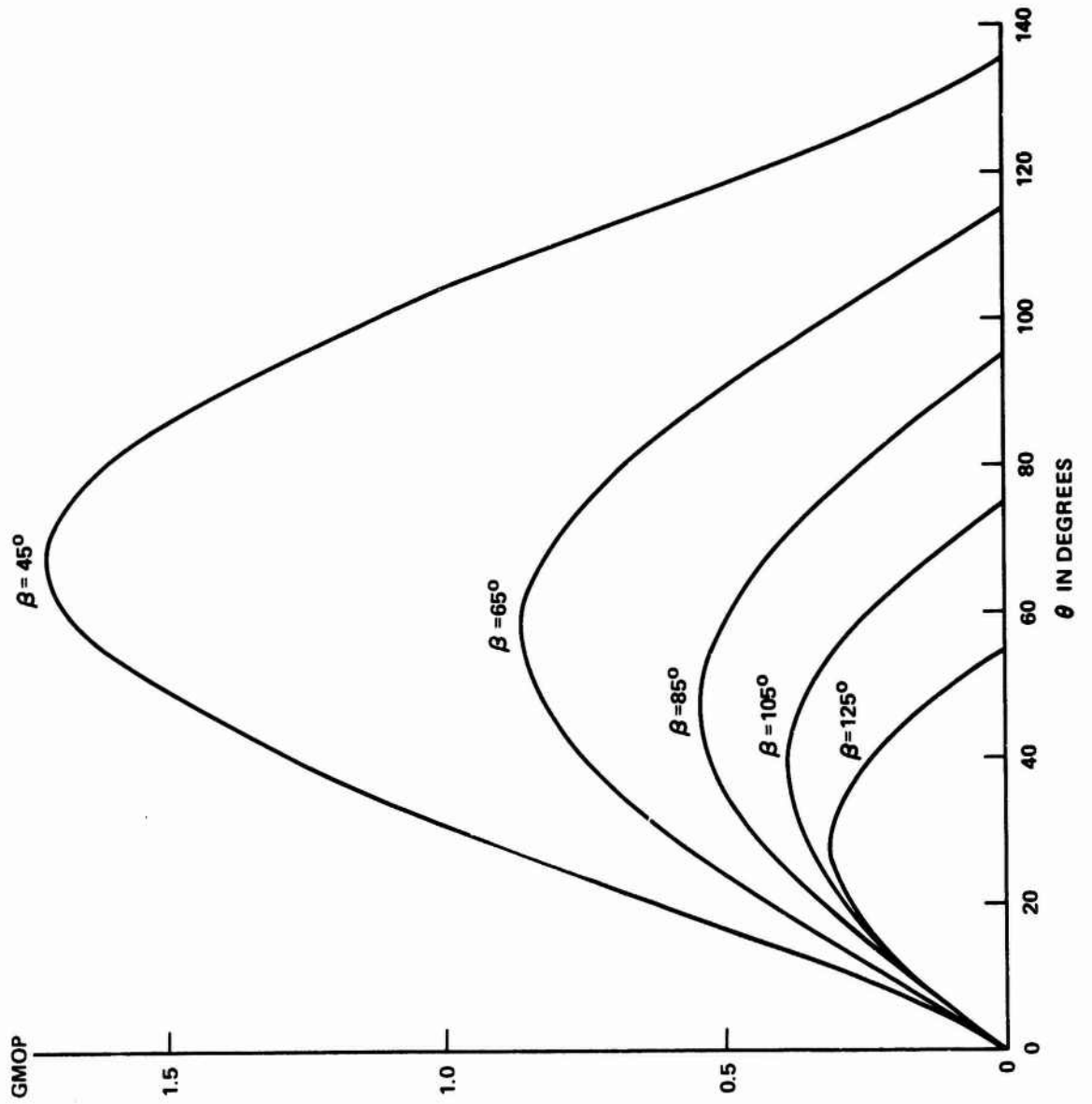


Figure 3-4b. Curves of GMOP vs. θ , for $\beta = 45^\circ, 65^\circ, 85^\circ, 105^\circ, 125^\circ$.

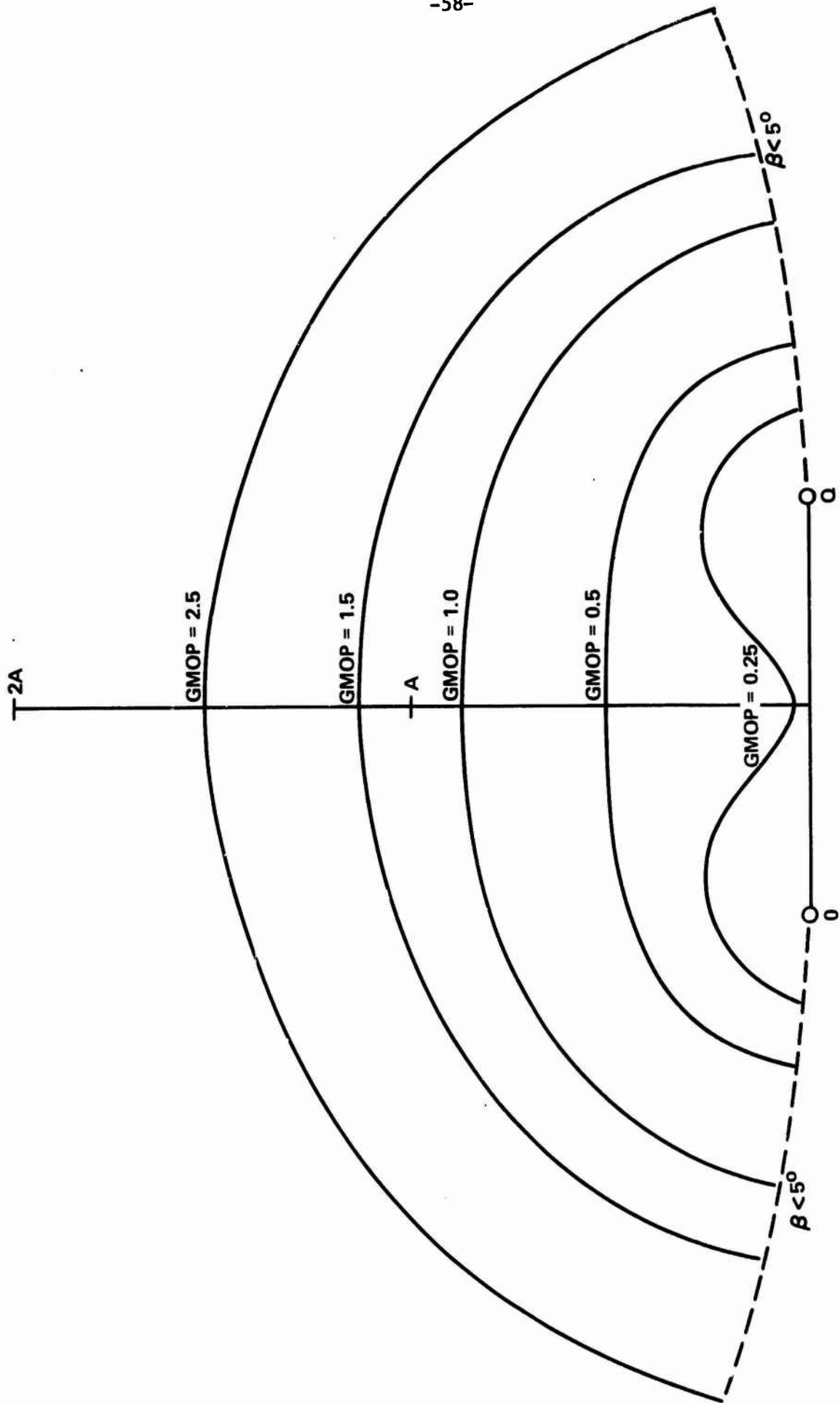


Figure 3-5. Contours of Constant GMOP Drawn to Scale
(Baseline OO of Length A)

interpolation in the second case requires that $\frac{\partial \text{GMOP}}{\partial \theta} \Big|_{\beta}$ is constant. Therefore, the behavior of each of these quantities is an indication of the accuracy which can be expected from linear interpolation for their respective cases. The equation of $\frac{\partial \text{GMOP}}{\partial \beta} \Big|_{\theta}$ is derived readily from eq. 3.9. The details of the derivation are shown in Appendix D. The result is

$$\frac{\partial \text{GMOP}}{\partial \beta} \Big|_{\theta} = -G \csc^3 \beta \left[\sin \beta \cos(\beta + \theta) + 2G \right] \quad (3.15)$$

where $G = \sin \theta$

Note that the quantity in brackets is a relatively "tame" function whose individual components never exceed a value of 2.0. The effect of this quantity is to modify the dominant $-\csc^3$ function. The degree of modification will depend upon the particular values of β and θ . The coefficient G exerts a more commanding influence of the shape of $\frac{\partial \text{GMOP}}{\partial \beta} \Big|_{\theta}$ in that the effect of the constant θ value is not diluted by the varying β values. Curves of $\frac{\partial \text{GMOP}}{\partial \beta} \Big|_{\theta}$ are shown in fig. 3-6. Although each curve exhibits constant (or nearly constant) $\frac{\partial \text{GMOP}}{\partial \beta} \Big|_{\theta}$ over some range of β , these ranges vary in size and position for different values of θ . In general, linear interpolation between curves of GMOP vs θ for constant incremental β is acceptable only over limited ranges of β which differ with changing θ .

The equation for $\frac{\partial \text{GMOP}}{\partial \theta} \Big|_{\beta}$ is taken from eq. 3.14 as

$$\frac{\partial \text{GMOP}}{\partial \theta} \Big|_{\beta} = 2E \sin(2\theta + \beta) \quad (3.16)$$

where $E = \frac{1}{2} \csc^2 \beta$

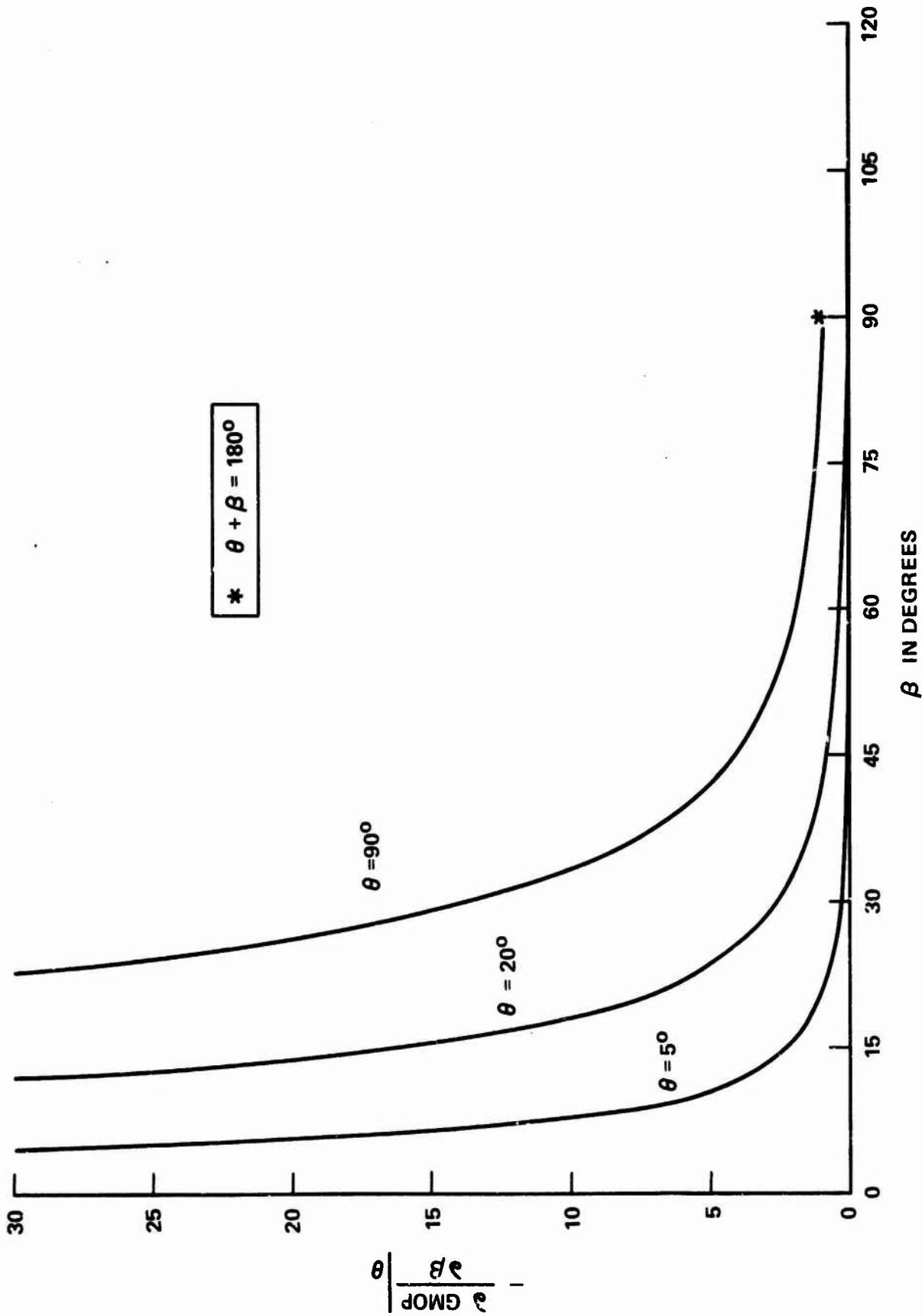


Figure 3-6. $-\frac{\partial \text{GMOP}}{\partial \beta}$ vs. β

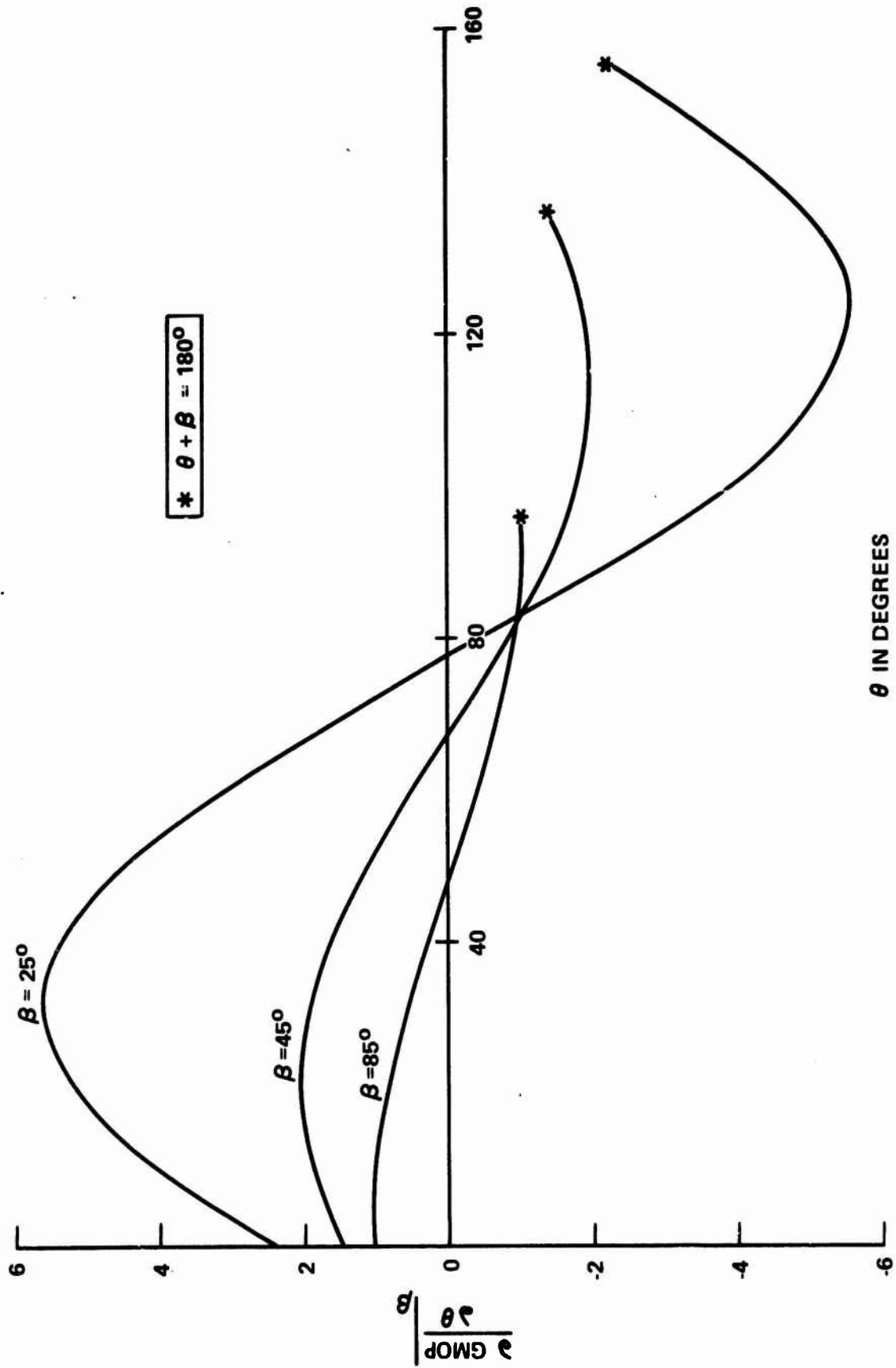


Figure 3-7. $\frac{\partial \text{GMOP}}{\partial \theta} \bigg|_{\beta}$ vs. θ

For any constant β , eq. 3.16 represents a sine curve of amplitude $\csc^2 \beta$. The most acceptable ranges of θ for linear interpolation purposes are those which include the section of the curve near a peak. Since the phase angle of the curves changes with β (the phase angle is, in fact, equal to β), these acceptable ranges will vary for varying β . Additionally, the amplitude of the curves varies inversely with β^* and, since a smaller amplitude will effect a "flatter" curve, the range of θ over which linear interpolation is acceptable increases with increasing β^* . Curves of $\left. \frac{\partial \text{GMOP}}{\partial \theta} \right|_{\beta}$ are presented in fig. 3-7. The results of figs. 3-6 and 3-7 prompt a general caution against linear interpolation. Until the acceptable error in GMOP is determined (as the error effects the calculation of σ_{1d} , σ_{2d} and μ_{12d}), it is advisable to calculate the required value for any specific case directly from eq. 3.9.

*for $0 \leq \beta \leq 90^\circ$

4. THE LOP CROSSING ANGLE (α)

4.1 The Calculation of α

This chapter is dedicated to the derivation and presentation of a method for calculating the LOP crossing angle α as an input to the basic method of determining the positioning accuracy developed in Section 2.3. The LOP crossing angle is defined as the acute angle between the tangents to the LOP's at the observer's position P (see fig. 2-1). It is shown physically for the respective cases of figs. 1-4 in figs. 4-1. The effect of α on the reliability of a position fix will not be addressed specifically in this report. (The deterioration of fix reliability with the deviation of α from 90° is demonstrated effectively in fig. 7 of ref. 2.)

Consider the illustration of one LOP in fig. 4-2. The development of Section 1.1 provides the value of $\angle COQ = \frac{\pi}{2} - \beta$ (point C is the center of the circular LOP). It follows from fig. 4-2 that

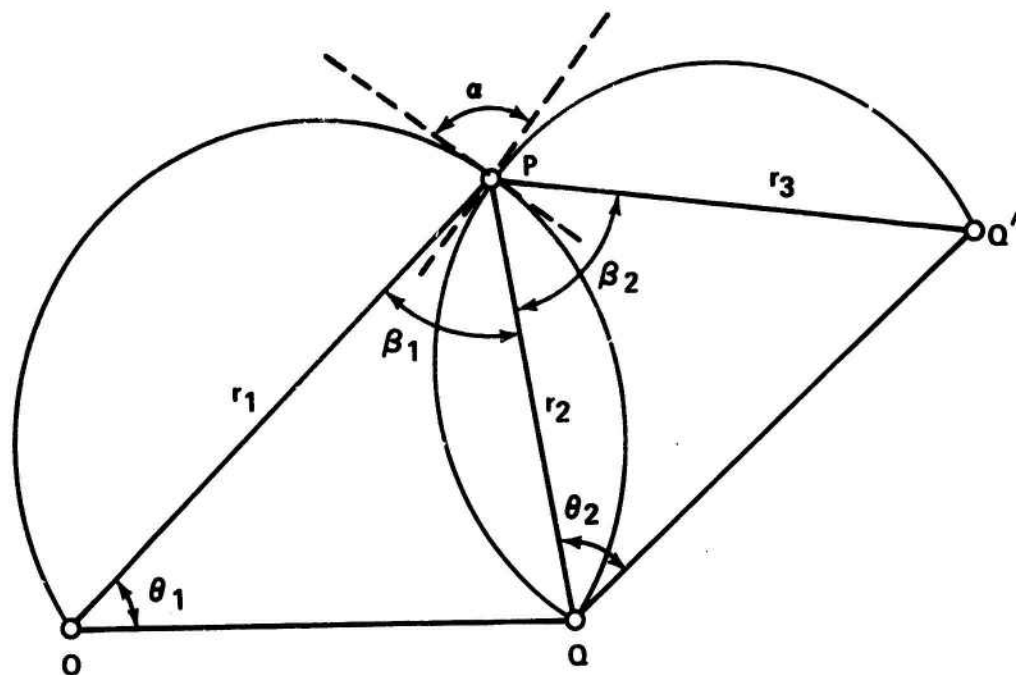
$$\eta = \theta - \angle COQ = \theta - \frac{\pi}{2} + \beta \quad (4.1)$$

Since $\triangle OPC$ is isosceles (two of its sides are radii of the circle), $\angle POC = \angle OPC$; and ψ in fig. 4-2 is given by

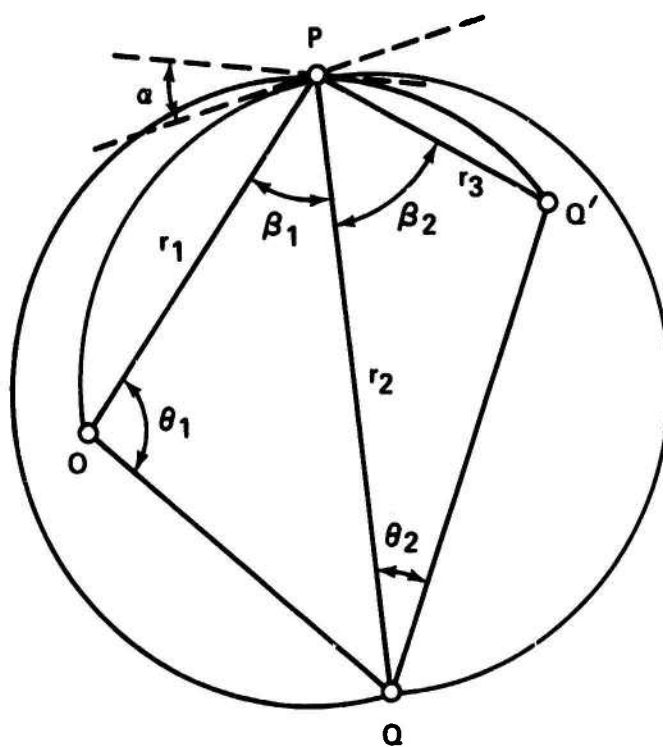
$$\psi = \frac{\pi}{2} + \eta = \theta + \beta \quad (4.2)$$

This expression for ψ can be derived readily for configurations encompassing all possible combinations of β and θ .

The two general configurations of the tangents to the LOP's and the position vectors \vec{r} at the observers' position P are shown for the case of fig. 4-1a in figs. 4-3. From fig. 4-3a,



a. Situation corresponding to fig. 1-4a.



b. Situation corresponding to fig. 1-4b.

Figure 4-1. Illustration of LOP crossing angles for the two general geometric cases of fig. 1-4.

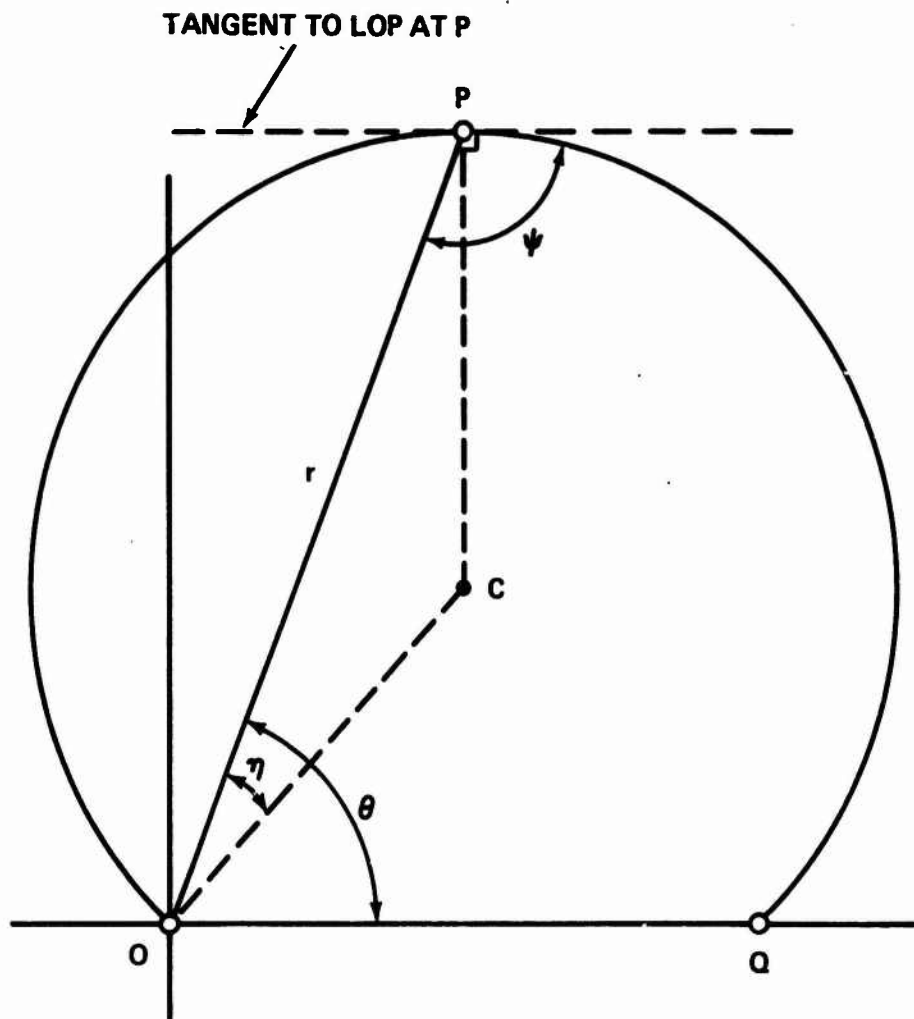


Figure 4.2 One LOP showing the angle ψ

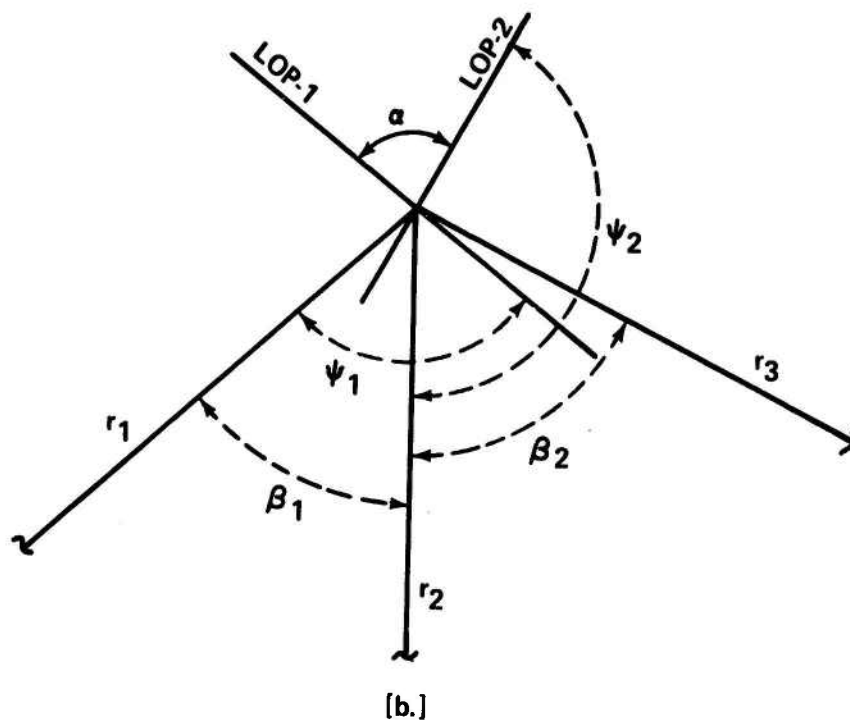
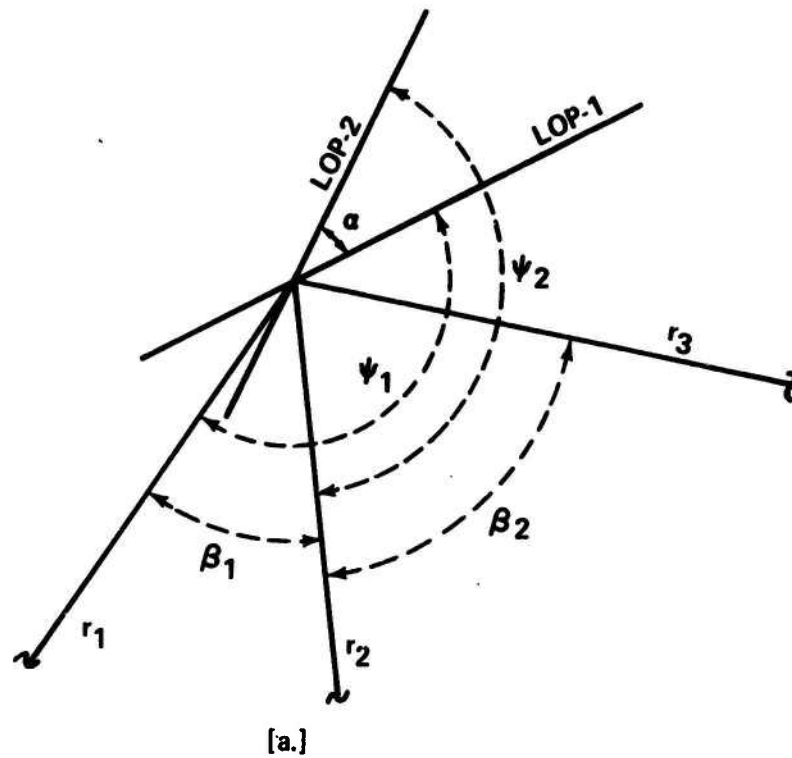


Figure 4-3. Geometric situations near the intersection of the LOP's for fig. 4-1a.

$$\alpha = \psi_2 - (\psi_1 - \beta_1) \quad (4.3)$$

Substituting eq. 4.2 into eq. 4.3 yields

$$\alpha = \theta_2 + \beta_2 - \theta_1 \quad (4.4)$$

In like manner, from fig. 4-3b,

$$\alpha = \pi - [\psi_2 - (\psi_1 - \beta_1)]$$

$$\text{or } \alpha = \pi - (\theta_2 + \beta_2 - \theta_1) \quad (4.5)$$

Figs. 4-4 show the two general configurations for the case of fig. 4-1b.

From fig. 4-4a,

$$\alpha = \psi_1 - (\psi_2 + \beta_1)$$

$$\text{or } \alpha = \theta_1 - \theta_2 - \beta_2 = -(\theta_2 + \beta_2 - \theta_1) \quad (4.6)$$

From fig. 4-4b,

$$\alpha = \pi - [\psi_1 - (\psi_2 + \beta_1)]$$

$$\text{or } \alpha = \pi - (\theta_1 - \theta_2 - \beta_2) = \pi - [-(\theta_2 + \beta_2 - \theta_1)] \quad (4.7)$$

Eqs. 4.4, 4.5, 4.6 and 4.7 can be used to form the general rule for determining the LOP crossing angle α , stated as follows:

$$\begin{aligned} \alpha &= \left| \theta_2 + \beta_2 - \theta_1 \right|, \quad \left| \theta_2 + \beta_2 - \theta_1 \right| \leq 90^\circ \\ \alpha &= 180^\circ - \left| \theta_2 + \beta_2 - \theta_1 \right|, \quad \left| \theta_2 + \beta_2 - \theta_1 \right| > 90^\circ \end{aligned} \quad (4.8)$$

where the absolute value of $(\theta_2 + \beta_2 - \theta_1)$ is taken to allow for the negative values of this quantity which are encountered for the case of

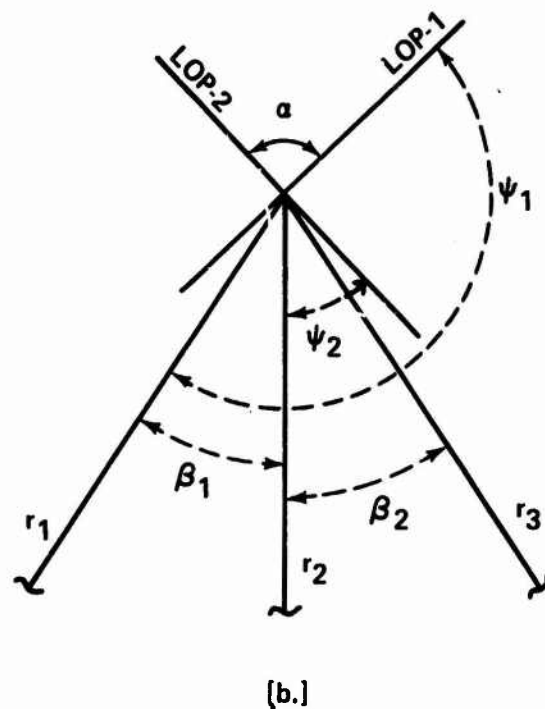
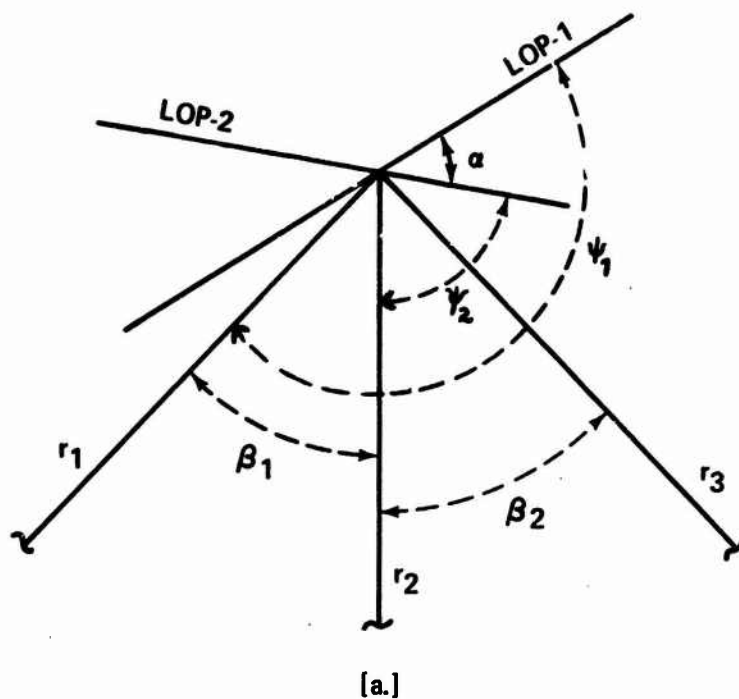


Figure 4-4. Geometric situations near the intersection of the LOP's for fig. 4-1b.

fig 4-1b (eqs. 4.6 and 4.7).

It should be noted that when $\alpha = 0$, the two horizontal sextant angles define the same LOP (fig. 4-5). This is called commonly a swing angle and is characterized by $\theta_2 + \beta_2 = \theta_1$. The disastrous implications of selecting objects which create this situation are apparent from fig. 4-5. The proper sextant angles can be measured from any point on the LOP. Also, note that eqs. 4.8 express α in terms of θ_2 , β_2 and θ_1 . Since these values are required for the calculation of GMOP (eq. 3.9), the determination of α involves very little additional effort.

The developments of this chapter along with those of Chapters 2 and 3 form the complete method for evaluating the accuracy of a position fix obtained from horizontal sextant angles. Since these developments are cluttered somewhat by the supporting theory, an example problem is provided in Chapter 5 to demonstrate the application of the complete method to a practical situation.

Additional Note: In order to apply rigorously the method for determining positioning accuracy developed herein, the proper absolute value and sign of the crossing angle α must be used. The absolute value of α is determined from eqs. 4.8. If α is measured from LOP-2 to LOP-1 in a counterclockwise direction (figs. 4-3b and 4-4a), the sign is positive; if measured from LOP-2 to LOP-1 in a clockwise direction (figs. 4-3a and 4-4b), the sign is negative. However, the sign of α affects both U_{12} (as defined for eqs. 2.31) and \mathcal{J} (eq. 2.33) directly. The manipulations of eqs. 2.35 neutralize the sign effects, i.e., the values of σ_x and σ_y calculated from eqs. 2.35 are unaffected by the sign of α . Consequently, to simplify the mechanics of applying the method, only positive α 's are used.

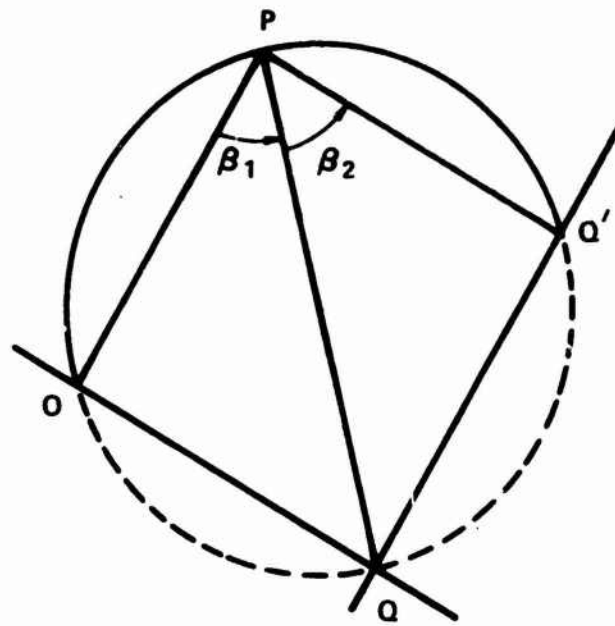


FIG. 4-5 A SWING ANGLE ($\alpha=0$)

5. AN EXAMPLE PROBLEM

5.1 The General Procedure

The developments of the preceding chapters can be combined now with the concepts of Appendix A to formulate the general step-by-step procedure for determining the accuracy of a horizontal sextant angle position fix.

The steps of the procedure are listed as follows:

Step 1: Determine the angular variances of the individual LOP's and the angular covariance of the combined LOP's using eqs. 2.11, 2.12 and 2.19.

$$\sigma_1^2 = \sigma_i^2 + \sigma_q^2 + \sigma_{p_1}^2 \quad (2.11)$$

$$\sigma_2^2 = \sigma_h^2 + \sigma_q^2 + \sigma_{p_2}^2 \quad (2.12)$$

$$\mu_{12} = - \sigma_{\theta_2}^2 - \sigma_q^2 \quad (2.19)$$

The definition of the component variances can be derived from the relationships established in chapters 1 and 2 and Appendix A. Consider first the variance σ_i^2 . The angular error ϵ_i is given in Chapter 2 as

$$\epsilon_i = \epsilon_o + \epsilon_r \quad (5.1)$$

As defined in Section 1.3, ϵ_o consists of the error in placing the arm PO directly through the center of point O (fig. 1-5) and the error in charting the position of the fixed object O. For the purposes of this example, it is assumed hereafter that the charted position of each of the points O, Q and Q' is exact. Therefore, ϵ_o consists solely of the error in placing the arm PO. The error ϵ_r is defined in Section 1.3 as the combination of the independent system errors including the three-arm protractor instrument

error and the sextant instrument and human errors. In equation form,

$$\epsilon_r = \epsilon_{3a} + \epsilon_{sti} + \epsilon_{sth} \quad (5.2)$$

where ϵ_{3a} is the three-arm protractor instrument error; ϵ_{sti} is the sextant instrument error; and ϵ_{sth} is the sextant human error.

Eq. 5.2 can be substituted into eq. 5.1 to give ϵ_i as

$$\epsilon_i = \epsilon_o + \epsilon_{3a} + \epsilon_{sti} + \epsilon_{sth} \quad (5.3)$$

Since each of the components ϵ_o , ϵ_{3a} , ϵ_{sti} and ϵ_{sth} are individually independent, eq. 5.3 can be used in eq. 2.8 to yield

$$\sigma_i^2 = E[\epsilon_i^2] = \sigma_o^2 + \sigma_{3a}^2 + \sigma_{sti}^2 + \sigma_{sth}^2 \quad (5.4)$$

Similarly,

$$\sigma_h^2 = E[\epsilon_h^2] = \sigma_{q'}^2 + \sigma_{3a}^2 + \sigma_{sti}^2 + \sigma_{sth}^2 \quad (5.5)$$

The variances $\sigma_{p_1}^2$ and $\sigma_{p_2}^2$ can be determined by using the expressions for ϵ_{p_1} and ϵ_{p_2} given in Appendix A as

$$\epsilon_{p_1} = \Delta\theta_2 - \Delta\theta_1 \quad (A.12)$$

$$\epsilon_{p_2} = -\Delta\theta_2 - \Delta\kappa_2 \quad (A.8)$$

in eq. 2.8. Since each of the angular changes $\Delta\theta_1$, $\Delta\theta_2$ and $\Delta\kappa_2$ are independent of any other single angular change, the results are

$$\sigma_{p_1}^2 = E[\epsilon_{p_1}^2] = \sigma_{\Delta\theta_2}^2 + \sigma_{\Delta\theta_1}^2 \quad (5.6)$$

$$\text{and } \sigma_{p_2}^2 = E[\epsilon_{p_2}^2] = \sigma_{\Delta\theta_2}^2 + \sigma_{\Delta\kappa_2}^2 \quad (5.7)$$

Now, substituting eqs. 5.4 through 5.7 into eqs. 2.11 and 2.12,

$$\sigma_1^2 = \sigma_o^2 + \sigma_{3a}^2 + \sigma_{sti}^2 + \sigma_{sth}^2 + \sigma_q^2 + \sigma_{\Delta\theta_2}^2 + \sigma_{\Delta\theta_1}^2 \quad (5.8)$$

and

$$\sigma_2^2 = \sigma_{q'}^2 + \sigma_{3a}^2 + \sigma_{sti}^2 + \sigma_{sth}^2 + \sigma_q^2 + \sigma_{\Delta\theta_2}^2 + \sigma_{\Delta K_2}^2 \quad (5.9)$$

Eqs. 5.8, 5.9 and 2.19 show completely the component variances of σ_1^2 , σ_2^2 and μ_{12} which will be considered for this example problem. The calculation of the values of the component variances is considered in Section 5.2.

Step 2: Determine \hat{K}_1 and \hat{K}_2 , the factors required to convert σ_1 , σ_2 and μ_{12} from angular units (radians) to distance units. Combining eqs. 3.1 and 3.9,

$$\hat{K} = (A)GMOP = A \sin \theta \csc \beta (\cos \theta + \cot \beta \sin \theta) \quad (5.10)$$

where A, θ and β are shown in fig. 3-2.

If the values of A_1 , θ_1 and β_1 for LOP-1 are substituted into eq. 5.10, the value of \hat{K}_1 is obtained; using A_2 , θ_2 and β_2 for LOP-2 produces \hat{K}_2 . It should be noted that hand calculations of \hat{K} can be facilitated by recognizing that

$$r = A(\cos \theta + \cot \beta \sin \theta) \quad (3.3)$$

so that

$$\hat{K} = r \sin \theta \csc \beta \quad (5.11)$$

where r is the distance from O to P for LOP-1 and from Q to P for LOP-2.

The variances and the covariances are converted to distance units as follows:

$$\begin{aligned}\sigma_{1d} &= \hat{k}_1 \sigma_1 \\ \sigma_{2d} &= \hat{k}_2 \sigma_2 \\ \mu_{12d} &= \hat{k}_1 \hat{k}_2 \mu_{12}\end{aligned}\tag{5.12}$$

Step 3: Calculate the LOP crossing angle α from eqs. 4.8

$$\begin{aligned}\alpha &= \left| \theta_2 + \beta_2 - \theta_1 \right|, \left| \theta_2 + \beta_2 - \theta_1 \right| \leq 90^\circ \\ \alpha &= 180^\circ - \left| \theta_2 + \beta_2 - \theta_1 \right|, \left| \theta_2 + \beta_2 - \theta_1 \right| > 90^\circ\end{aligned}\tag{4.8}$$

Step 4: Use σ_{1d} , σ_{2d} , μ_{12d} from eqs. 5.12 and α from eqs. 4.8 in the expressions for σ_{E_1} , σ_{E_2} , U_{12} and ρ_1 as they are defined for eq. 2.31.

$$\begin{aligned}\sigma_{E_1} &= \sigma_{1d} \\ \sigma_{E_2} &= \frac{1}{|\tan \alpha|} \sqrt{\sigma_{1d}^2 + \sigma_{2d}^2 \sec^2 \alpha - 2\mu_{12d} \sec \alpha} \\ U_{12} &= -\frac{1}{\tan \alpha} (\sigma_{1d}^2 - \mu_{12d} \sec \alpha) \\ \rho_1 &= \frac{U_{12}}{\sigma_{E_1} \sigma_{E_2}} = \frac{\sigma_{1d}^2 - \mu_{12d} \sec \alpha}{\sigma_{1d} \sqrt{\sigma_{1d}^2 + \sigma_{2d}^2 \sec^2 \alpha - 2\mu_{12d} \sec \alpha}}\end{aligned}\tag{5.13}$$

Step 5: Calculate the angle of axis rotation ρ from eq. 2.13.

$$\rho = \frac{1}{2} \tan^{-1} \left[\frac{2\rho_1 \sigma_{E_1} \sigma_{E_2}}{\sigma_{E_1}^2 - \sigma_{E_2}^2} \right]\tag{2.33}$$

Step 6: Calculate σ_x and σ_y by using the values of σ_{E_1} , σ_{E_2} and U_{12} obtained from eqs. 5.13 and the value of ρ from eq. 2.33 in eqs. 2.35.

$$\sigma_x = \sqrt{\sigma_{E_1}^2 \cos^2 \rho + \sigma_{E_2}^2 \sin^2 \rho + 2 U_{12} \sin \rho \cos \rho} \quad (2.35)$$

$$\sigma_y = \sqrt{\sigma_{E_1}^2 \sin^2 \rho + \sigma_{E_2}^2 \cos^2 \rho - 2 U_{12} \sin \rho \cos \rho}$$

Step 7: Enter the curves of fig. 2-3 with the smaller of the ratios $\frac{\sigma_x}{\sigma_y}$ or $\frac{\sigma_y}{\sigma_x}$ and the desired accuracy probability to obtain a value of K. The radius of the circular probability density contour, whose center is the center of the black dot used to mark the charted buoy anchor position, within which the particular horizontal sextant angle position fix can be expected to be for the particular accuracy probability is calculated using eq. 2.36.

$$R = K \sigma_b \quad (2.36)$$

where σ_b is the larger of σ_x and σ_y .

It can be seen that hand calculations of the positioning accuracy for any particular problem are relatively long and tedious. However, the method does lend itself nicely to computer programming, where the parameters peculiar to the problem would be the required inputs. Many calculations could be handled by a computer in a short time. Nevertheless, a sample hand calculation will be carried out in Section 5.3 to illustrate the mechanics of using the step-by-step procedure.

5.2 Probabilistic Variable Definitions

This section addresses the problem of defining the means of calculating the component variances of σ_1^2 , σ_2^2 and μ_{12} , shown in eqs. 5.8, 5.9 and 2.19. The reader is referred to Appendix A for the derivation of the equations which express ϵ_o , ϵ_q , $\epsilon_{q'}$, $\Delta\theta_1$, $\Delta\theta_2$ and $\Delta\kappa_2$ in terms of measurable distance errors in placing the three-arm protractor arms directly through the centers of O, Q and Q' and in placing the pivot point directly over P. Applying eqs. 2.8 and the implication of eqs. 2.23 and 2.24 to eqs. A.1, A.2, A.3, A.6, A.9 and A.10 yields

$$\sigma_o^2 = \frac{\sigma_{y_1}^2}{r_1^2},$$

$$\sigma_q^2 = \frac{\sigma_{y_2}^2}{r_2^2},$$

$$\sigma_{q'}^2 = \frac{\sigma_{y_3}^2}{r_3^2}, \quad (5.14)$$

$$\sigma_{\Delta\theta_1}^2 = \frac{\sigma_{s'_1}^2}{r_1^2},$$

$$\sigma_{\Delta\theta_2}^2 = \frac{\sigma_{t_2}^2}{r_2^2},$$

and
$$\sigma_{\Delta k_2}^2 = \frac{\sigma_u^2}{r_3^2}$$

where r_1 , r_2 and r_3 are the lengths PO, PQ and PQ' respectively. Limited experimental results from twelve samples of each variable taken by two subjects indicate that it is reasonable to assume the following:

- a. The distributions of y_1 , y_2 and y_3 are identical. Each approximates a uniform distribution which is symmetrical about the center of the black dot used to chart the position of the particular fixed object. Further, it seems that the human mind can edit possible error positions of O, Q and/or Q' which lie beyond the limits of a circle whose center is that of the black dot but whose diameter is equivalent to that of the smallest black dot used to chart the positions of fixed objects ashore (approximately 0.01 inch on all NOS charts).
- b. The error points P_e (figs. A-3 and A-4) have a circular uniform distribution about the center of the black dot used to chart the buoy anchor position. Again, error points outside a circle of diameter equal to that of the small black dot used to chart the positions of fixed objects ashore seem to be eliminated. Consequently, the diameter of the circular distribution is approximately equal to that of the small black dot.

Therefore, the variances on the right-hand sides of eqs. 5.14 are equal.

The standard deviation of the uniformly distributed variables is defined by

$$\sigma = \frac{d}{\sqrt{12}} \quad (5.15)$$

where d is the diameter of the small black dot.

Using 0.01 inch as the value of d and generalizing eq. 5.15 for any chart scale factor N ,

$$\sigma = \frac{(0.01)N}{(12)(\sqrt{12})} = (2.4 \times 10^{-4})N \quad (5.16)$$

where σ is in feet.

This expression for σ can be used in each of the eqs. 5.14 to determine the indicated component variances. However, it must be emphasized that eq. 5.16 is an expression for σ which is based upon assumptions made from very limited data. Its accuracy will remain suspect until it is substantiated by much more experimental data.

Preliminary experimental results presented in ref. 7 indicate that the standard deviation of the human error in measuring angles using the sextant is approximately 6'05.5". It will be assumed for the purposes of this example problem that

$$\sigma_{sth} = 6'05.5" = 17.7 \times 10^{-4} \text{ radians} \quad (5.17)$$

Assuming that the sextants used are adjusted perfectly, the instrument error in measuring angles with the sextant is due to the limited precision of the instrument. A general assumption which is made to approximate the expected error due to this limited precision, called the granularity, is that the error is uniformly distributed between the smallest graduations on the instrument. Usually, sextants offer marked precision to the nearest

tenth of a minute. Therefore,

$$\sigma_{sti} = \frac{(0.1)}{(60)(57.3)(\sqrt{12})} = 0.084 \times 10^{-4} \text{ radians} \quad (5.18)$$

Similarly, since the most commonly used three-arm protractors are marked to two minutes of arc,

$$\sigma_{3a} = \frac{2}{(60)(57.3)(\sqrt{12})} = 1.7 \times 10^{-4} \text{ radians} \quad (5.19)$$

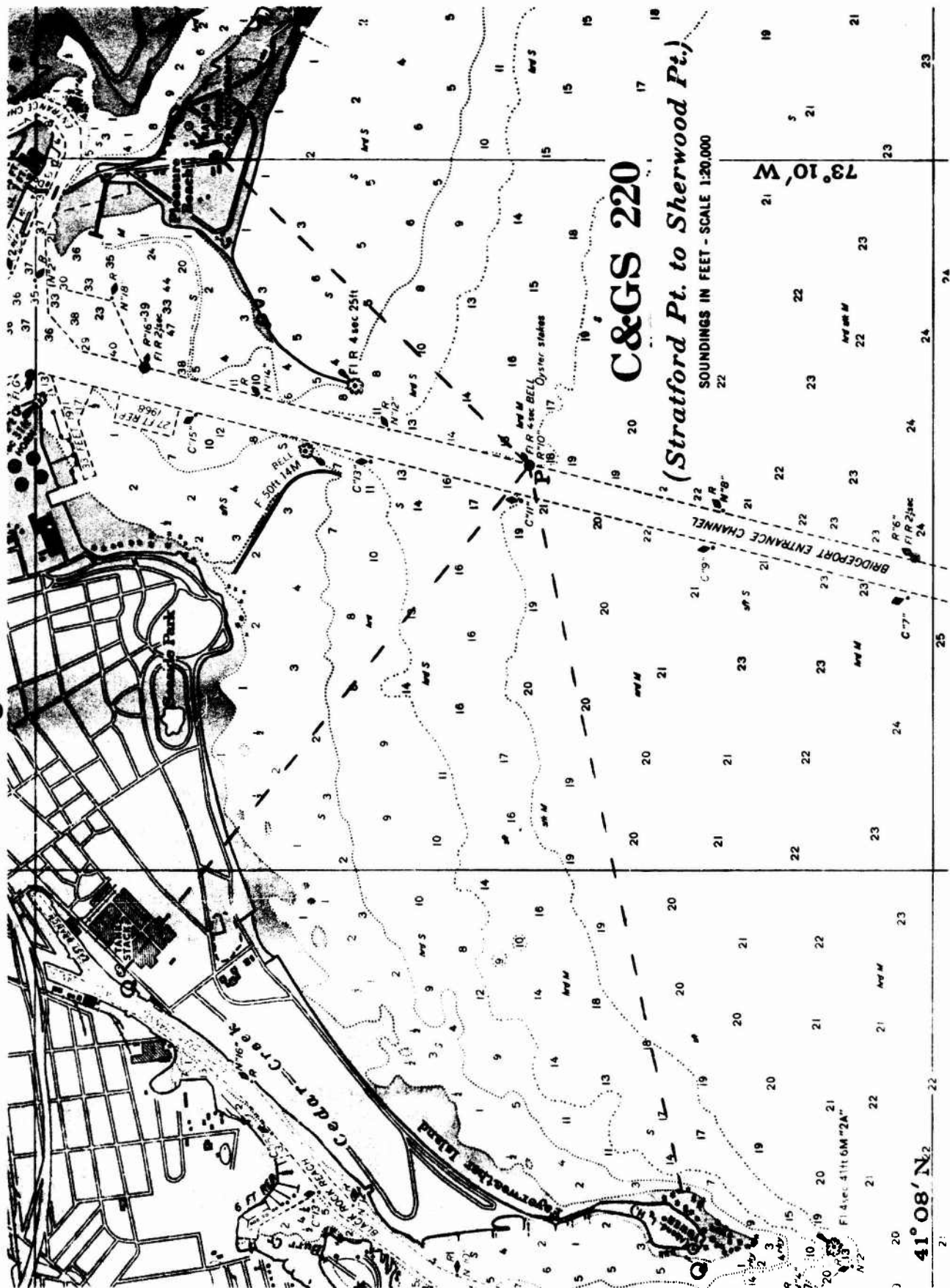
Eqs. 5.14, 5.16, 5.17, 5.18 and 5.19 define all of the component variances of σ_1^2 , σ_2^2 and μ_{12} for the purposes of the example problem.

5.3 The Actual Problem

The problem which will be presented to illustrate the application of the method for determining positioning accuracy which is derived in this report is that of positioning the anchor of Bridgeport Entrance Lighted Bell Buoy #10. A portion of C&GS (now NOS) chart #220 which includes the buoy anchor position, labeled P, and the labeled fixed objects O, Q and Q' is shown in fig. 5-1. The following parameters are taken from the chart:

$N = 20,000$	$r_1 = 6450 \text{ ft}$
$\beta_1 = 92^{\circ}12'$	$r_2 = 8400 \text{ ft}$
$\beta_2 = 52^{\circ}32'$	$r_3 = 10,050 \text{ ft}$
$\theta_1 = 50^{\circ}06'$	$A_1 = 10,800 \text{ ft}$
$\theta_2 = 74^{\circ}44'$	$A_2 = 8400 \text{ ft}$

Fig. 5-1



Step 1: Using eq. 5.16,

$$\sigma = (2.4 \times 10^{-4})(N) = 4.8 \text{ ft}$$

Substituting this value into eqs 5.14 yields

$$\sigma_o^2 = \sigma_{\Delta\theta_1}^2 = \left(\frac{4.8}{6450}\right)^2 = 55.4 \times 10^{-8} \text{ radians}$$

$$\sigma_q^2 = \sigma_{\Delta\theta_2}^2 = \left(\frac{4.8}{8400}\right)^2 = 32.7 \times 10^{-8} \text{ radians}$$

$$\sigma_{q'}^2 = \sigma_{\Delta K_2}^2 = \left(\frac{4.8}{10,050}\right)^2 = 22.8 \times 10^{-8} \text{ radians}$$

Using these values and those of eqs. 5.17, 5.18 and 5.19 in eqs. 5.8, 5.9 and 2.19 yields

$$\sigma_1 = 22.2 \times 10^{-4} \text{ radians}$$

$$\sigma_2 = 20.7 \times 10^{-4} \text{ radians}$$

$$\mu_{12} = - 65.4 \times 10^{-8} \text{ radians}^2$$

Step 2: Using eq. 5.10,

$$\hat{K}_1 = 5030.5 \text{ ft/radian}$$

$$\hat{K}_2 = 10,237.0 \text{ ft/radian}$$

Eqs. 5.12 can be used to obtain

$$\sigma_{1d} = 11.2 \text{ ft}$$

$$\sigma_{2d} = 21.2 \text{ ft}$$

$$\mu_{12d} = - 33.7 \text{ ft}^2$$

Step 3: Using eqs. 4.8,

$$\alpha = 76.2^{\circ}$$

Step 4: Substituting $\sigma_{1d}, \sigma_{2d}, \mu_{12d}$ and α into eqs. 5.13 yields

$$\sigma_{E_1} = 11.2 \text{ ft}$$

$$\sigma_{E_2} = 22.4 \text{ ft}$$

$$U_{12} = -65.5 \text{ ft}^2$$

$$\rho_1 = -0.26$$

Step 5: Use eq. 2.33 to find

$$\beta = 9.6^{\circ}$$

Step 6: Calculate σ_x and σ_y using eqs. 2.35 as

$$\sigma_x = 10.7 \text{ ft}$$

$$\sigma_y = 22.6 \text{ ft}$$

Step 7: $\frac{\sigma_x}{\sigma_y} < \frac{\sigma_y}{\sigma_x}$ so fig. 2-3 is entered with $\frac{\sigma_x}{\sigma_y} = 0.47$ and the

desired accuracy probability of 95% to obtain

$$K = 2.025$$

Using eq. 2.36, the radius from the center of the black dot within which the sinker can be expected to be placed for a 95% accuracy probability is

$$R = 45.8 \text{ ft}$$

This step-by-step procedure can be used in like manner to find the positioning accuracy for any other problem.

REFERENCES

1. Wells, Webster, The Elements of Geometry, (Leach, Shewell, and Sanborn)
2. Burt, W. Allan, et al, "Mathematical Considerations Pertaining to the Accuracy of Position Location and Navigation Systems - Part 1", Stanford Research Institute, April 1966, Distributed by NTIS AD 629 609
3. Baltzer, O. J., E. C. Fraser, et al, "River and Harbor Aid to Navigation System (RIHANS) Phase 1 - T: Systems Definition", Coast Guard Report No. CG-D-24-74, August 1973
4. Parzen, Emanuel, Modern Probability Theory and Its Applications, (John Wiley and Sons, 1960)
5. Hildebrand, Francis B., Advanced Calculus for Applications, ed. Dr. Albert A. Bennett (Prentice-Hall, 1962)
6. The Chemical Rubber Co., C. R. C. Standard Mathematical Tables, Thirteenth Edition, ed. in chief Robert C. Weast, Ph.D.
7. Goodwin, E. M. and J. F. Kemp, "Accuracy Contours for Horizontal Angle Position Lines", The Journal of Navigation, Vol. 26, No. 4, October 1973, pp. 481-485
8. Cotter, Charles H., "A Brief History of the Method of Fixing by Horizontal Angles", The Journal of Navigation, Vol. 25, No. 4, October 1972, pp. 528-533

APPENDIX A

The discussion of error sources in Section 1.3 presents the errors in measuring the horizontal sextant angles using the three-arm protractor as angular errors which modify the exact angular measurements. These errors result from the improper placement of the protractor arms PO, PQ and PQ' (fig. 1-5) and the improper placement of the pivot point over the point (observer's position) P*. This appendix addresses the problem of defining the statistical distribution relationships of the angular errors to measureable distance errors due to the use of the three-arm protractor. These distributions are necessary to determine some of the variances and the covariances used in the development of Section 2.3.

Consider first the angular errors ϵ_o , ϵ_q and $\epsilon_{q'}$, which result from the improper placement of arms PO, PQ and PQ'. If the protractor pivot point is fixed directly over the point P and the center arm PQ is positioned through point Q, all of the angular error will be contributed by the incorrect placement of the arm. Fig. A-1 shows the exact placement of the arm PQ and a hypothetical incorrect placement PQ_e. The vector \vec{y}_2 is constructed from PQ to PQ_e, perpendicular to PQ at Q. Assuming that the error point Q_e is always within the small black dot with which the position of an object is charted, the magnitude y_2 is always much smaller than the length PQ. Consequently, ϵ_q is small and

$$\epsilon_q = \tan^{-1}\left(\frac{y_2}{r_2}\right) \approx \frac{y_2}{r_2} \quad (A.1)$$

where y_2 and r_2 are shown in fig. A-1 and ϵ_q is in radians.

*It is assumed that the charted position of each of the points O, Q and Q' is exact.

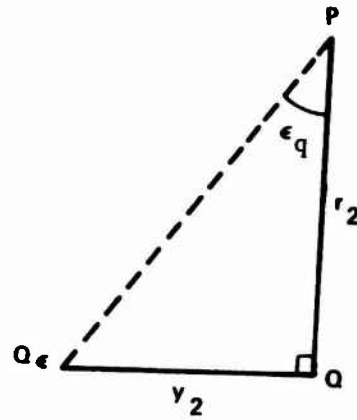


FIG. A-1 THE ERROR IN PLACING ARM PQ THROUGH THE CENTER OF Q

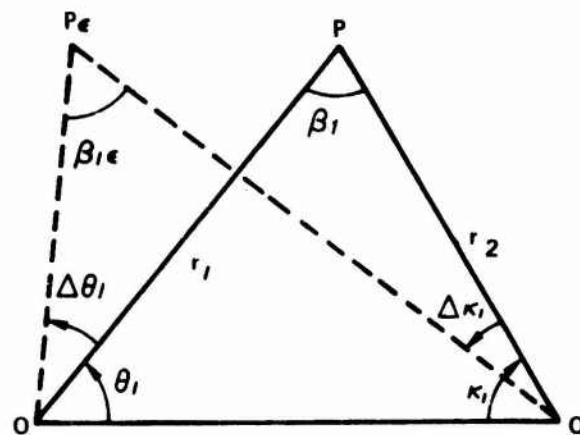


FIG. A-2 THE ERRORS AFFECTING β , DUE TO THE INCORRECT PLACEMENT OF PIVOT POINT OVER P

Eq. A.1 implies that the distribution of ϵ_q can be specified completely by the one-dimensional distribution of y_2 divided by r_2 . Note that r_2 is constant for any particular problem. Similarly, the distributions of ϵ_o and ϵ_q' are defined by

$$\epsilon_o \approx \frac{y_1}{r_1} \quad (A.2)$$

$$\text{and } \epsilon_q' \approx \frac{y_3}{r_3} \quad (A.3)$$

where y_1 and y_3 are the magnitudes of the \vec{y} vectors from PO and PQ' to PO_{ϵ} and PQ'_{ϵ} , perpendicular at O and Q' respectively; and r_1 and r_3 are the lengths PO and PQ'.

The determination of practical expressions for ϵ_{p_1} and ϵ_{p_2} is a more complicated problem. If the arms PO, PQ and PQ' are fixed through the centers of O, Q and Q', all of the angular error is due to the improper placement of the pivot point over point P. Fig. A-2 shows the effect of the error on the measurement of $\angle OPQ$. The incorrect placement of the pivot point changes the orientations of arms PO and PQ which causes the angular changes $\Delta\theta_1$ and $\Delta\kappa_1$. Since the sum of the three angles must remain 180° , the measured value of the horizontal sextant angle may be affected also. The angular effect on β_1 is designated ϵ_{p_1} ; in fig. A-2, $\beta_{1\epsilon} = \beta_1 + \epsilon_{p_1}$, where the sign of ϵ_{p_1} depends on the situation. So,

$$\beta_1 + \epsilon_{p_1} + \theta_1 + \Delta\theta_1 + \kappa_1 + \Delta\kappa_1 = 180^\circ \quad (A.4)$$

where the signs of $\Delta\theta_1$ and $\Delta\kappa_1$ also depend on the situation.

But $\beta_1 + \theta_1 + \kappa_1 = 180^\circ$

Therefore, eq. A.4 reduces to

$$\epsilon_{p_1} + \Delta\theta_1 + \Delta\kappa_1 = 0$$

$$\text{or } \epsilon_{p_1} = -(\Delta\theta_1 + \Delta\kappa_1) \quad (\text{A.5})$$

Eq. A.5 implies that the distribution of ϵ_{p_1} can be derived from the distributions of $\Delta\theta_1$ and $\Delta\kappa_1$. The distributions of $\Delta\theta_1$ and $\Delta\kappa_1$ can be determined using the method by which ϵ_o , ϵ_q and $\epsilon_{q'}$ were defined. In fig. A-3 vector \vec{s} is constructed from PO to P_e O, perpendicular to PO at P. Since $\Delta\theta_1$ is small,

$$\Delta\theta_1 \cong \frac{s'}{r_1} \quad (\text{A.6})$$

where r_1 is the length PO.

Similarly, if \vec{t} is constructed from PQ to P_e Q, perpendicular to PQ at P (fig. A-3),

$$\Delta\kappa_1 \cong \frac{-t}{r_2} \quad (\text{A.7})$$

where r_2 is the length PQ.

The distribution for the angular error in the measurement of $\angle QPQ'$ due to the improper placement of the protractor pivot point can be derived from fig. A-4 as

$$\epsilon_{p_2} = -(\Delta\theta_2 + \Delta\kappa_2) \quad (\text{A.8})$$

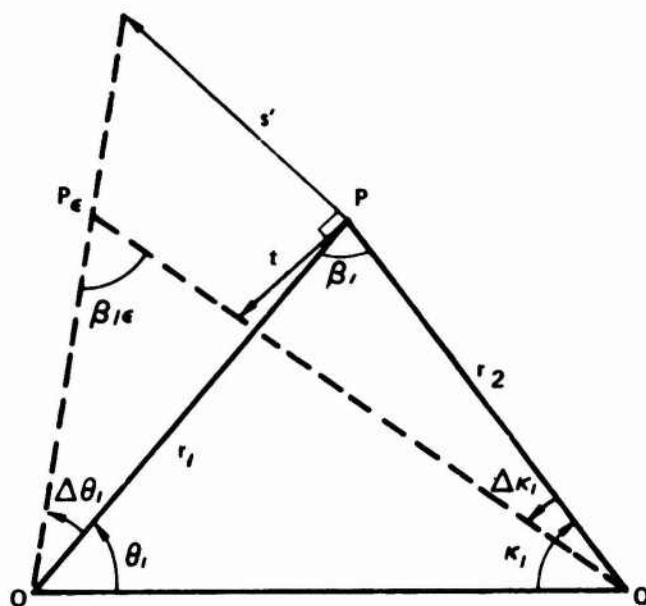


FIG. A-3 DEFINING THE ANGULAR CHANGES $\Delta\kappa_1$ AND $\Delta\theta_1$

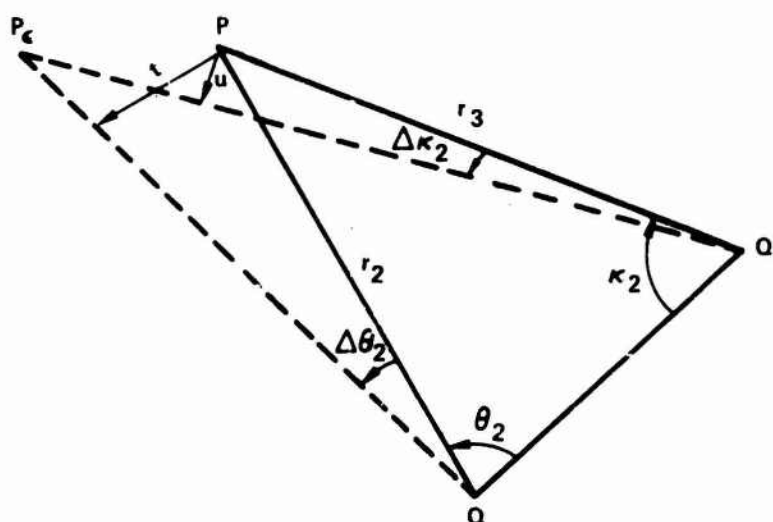


FIG. A-4 DEFINING THE ANGULAR CHANGES $\Delta\theta_2$ AND $\Delta\kappa_2$

$$\text{where } \Delta\theta_2 \cong \frac{t}{r_2} \quad (\text{A.9})$$

$$\text{and } \Delta\kappa_2 \cong \frac{-u}{r_3} \quad (\text{A.10})$$

Notice that $\angle OQQ' = \kappa_1 + \theta_2$. Since the arms are fixed through the centers of their respective points, $\angle OQQ'$ is constant and any change in θ_2 creates an equal and opposite change in κ_1 or

$$\theta_2 = -\kappa_1 \quad (\text{A.11})$$

Eqs. A.7 and A.9 reflect this relationship. Substituting eq. A.11 into eq. A.5,

$$\epsilon_{p_1} = \Delta\theta_2 - \Delta\theta_1 \quad (\text{A.12})$$

Eqs. A.12 and A.8 are expressions which define the distributions of ϵ_{p_1} and ϵ_{p_2} . The distributions of the components are defined by eqs. A.6, A.9 and A.10. The important implication of this appendix is that, if the one-dimensional distributions of y_1 , y_2 and y_3 are symmetrical about the centers of the black dots used to chart the positions of the fixed objects and if the distribution of the error points P_e (figs. A-3 and A-4) about the center of the black dot used to chart the position of the buoy anchor is circular, suitable samples of y_1 , y_2 , y_3 , s' , t and u taken from one experiment can be used to determine the distributions (and the values of the probabilistic variables) of the angular errors ϵ_o , ϵ_q and $\dot{\epsilon}_q$, and the angular changes $\Delta\theta_1$, $\Delta\theta_2$ and $\Delta\kappa_2$, which define ϵ_{p_1} and ϵ_{p_2} . The probabilistic variables describing these errors are necessary for the implementation of the method for determining positioning accuracy.

APPENDIX B

Assumption "d" of Section 2.1, made with reference to fig. 2-1, is restated for convenience as follows:

in the neighborhood of the observers' position P,

- d. the LOP's approximate straight lines and the angular errors ϵ can be transformed into distance errors measured along a straight line which is perpendicular to the exact LOP and the error LOP.

It is the purpose of this appendix to present the analysis which proves the general acceptability of this assumption. As stated in ref. 2, the LOP's approximate straight lines in the neighborhood of P if the radius of curvature of the exact LOP is much larger than the one - σ error (in distance units). This requirement is represented in equation form as

$$\frac{\hat{R}}{\sigma_d} \gg 1 \quad (B.1)$$

where \hat{R} is the radius of the exact circular LOP and σ_d is the standard deviation of the random error in distance units.

Fig. B-1 is a reconstruction of fig. 1-3a which includes additionally some angular and linear measurements derived in Section 1.1. From this figure it can be seen that

$$\hat{R} = \frac{1}{2} A \csc \beta \quad (B.2)$$

The combination of eqs. 3.1 and 3.9 yields

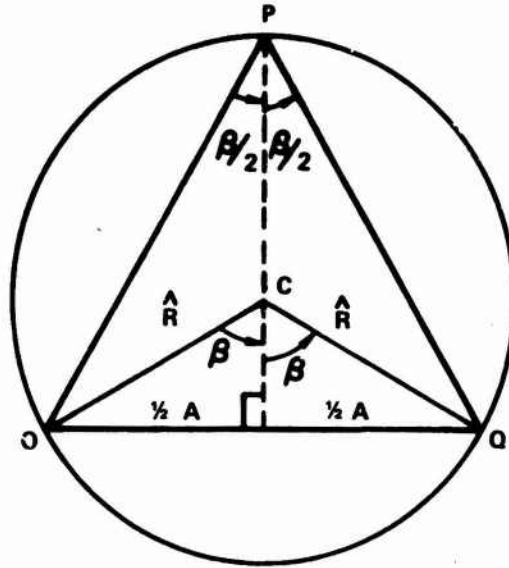


FIG. B-1 RECONSTRUCTION OF FIG. 1-3a SHOWING
ADDITIONAL ANGULAR AND LINEAR
MEASUREMENTS

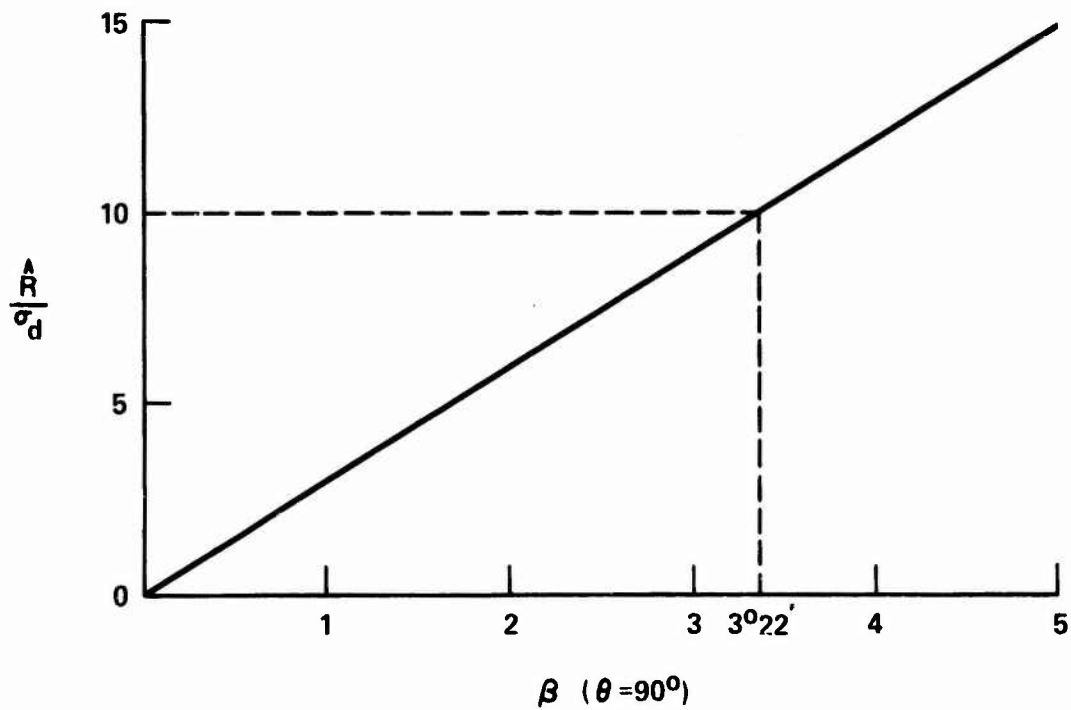


Figure B-2. Graphic Representation of Equation B.5 for $0 \leq \beta \leq 5^\circ$.

$$\sigma_d = A \sin \theta \csc \beta (\cos \theta + \cot \beta \sin \theta) \sigma_a \quad (B.3)$$

Now, eq. B.2 can be divided by B.3 to give

$$\frac{\hat{R}}{\sigma_d} = \frac{1}{2 \sin \theta (\cos \theta + \cot \beta \sin \theta) \sigma_a} \quad (B.4)$$

Preliminary indications are that $\sigma_a \sim 10$ minutes; therefore, $\sigma_a = 3 \times 10^{-3}$ radians will be assumed for the purposes of this analysis. The smallest values of $\frac{\hat{R}}{\sigma_d}$ will be encountered when the denominator of eq. B.4 is very large. It can be seen that the trigonometric functions of θ in eq. B.4 are very "tame", i.e., none of them will ever exceed the value of 1.0. Since σ_a is considered constant, the volatile term is $\cot \beta$ which will approach infinity as β approaches zero. For small values of β ($0 \leq \beta \leq 5^\circ$), setting θ to 90° will permit a clear view of the worst situations which can be expected, identifying different areas over the range of β from zero to five degrees for which eq. B.1 may not be satisfied. If $\theta = 90^\circ$, eq. B.4 may be rewritten as

$$\left(\frac{\hat{R}}{\sigma_d}\right)_\theta = \frac{\pi}{2} = \frac{\tan \beta}{2 \sigma_a} \approx (1.7 \times 10^2) \tan \beta \quad (B.5)$$

Fig. B-2 is the graphic representation of eq. B.5 for $0 \leq \beta \leq 5^\circ$. It can be seen from this figure that, if $\frac{\hat{R}}{\sigma_d} \geq 10$ is considered sufficient to satisfy the implication of eq. B.1, the first part of assumption "d" is acceptable for $\beta \geq 3^\circ 22'$. It should be noted that this result implies the acceptability of the assumption of linear LOP's in the neighborhood of P for all possible values of θ corresponding to any β greater than or

equal to $3^{\circ}22'$ (the upper limit on β is the maximum angle which can be measured by the sextant - 126° for the newest sextants). However, it does not preclude the acceptability of this assumption for some possible values of θ corresponding to β 's less than $3^{\circ}22'$. In fact, there is some θ which yields $\frac{\hat{R}}{\sigma_d} \geq 10$ for every possible value of β except $\beta = 0$. The logical conclusion is that, in general, the first part of assumption "d" is acceptable.

The second part of assumption "d" is acceptable if the radius of curvature of the particular curve of $\vec{\nabla}\beta$ along which the error is measured is much larger than the one σ error (in distance units). The logic of this statement can be seen intuitively from the representation of the contours of constant β and the curves of $\vec{\nabla}\beta$ shown in fig. 3-1. Unfortunately, the definition of the radius of curvature of the $\vec{\nabla}\beta$ curves is not readily apparent from the figure. In order to verify the shape and determine the expression for the radius of curvature of these curves, it is most useful to develop a scalar expression, similar to eq. 3.4, which describes the whole family of $\vec{\nabla}\beta$ curves. To accomplish this, the property of the mutual orthogonality of the contours of constant β and the $\vec{\nabla}\beta$ curves is exploited. By the definition of the gradient, there is some function ϕ which is constant on the $\vec{\nabla}\beta$ curves and for which the contours of constant β are the gradient curves. This concept is analogous to the velocity potential-stream function relationship of fluid dynamics or the potential-flux relationship of electromagnetic theory. The fact that $\vec{\nabla}\beta \cdot \vec{\nabla}\phi = 0$ everywhere is used in the form of the Cauchy-Riemann equations (ref. 5) in polar coordinates.

These are stated as follows:

$$\frac{\partial \phi}{\partial r} = - \frac{1}{r} \frac{\partial \beta}{\partial \theta} \quad (B.6)$$

and $\frac{1}{r} \frac{\partial \phi}{\partial \theta} = \frac{\partial \beta}{\partial r}$

Eqs. B.6 can be used to find the function ϕ from eq. 3.4. The form of $\frac{1}{r} \frac{\partial \beta}{\partial \theta}$ which is most useful in this case is given by eq. C.5. As it is stated in Appendix C,

$$\frac{1}{r} \frac{\partial \beta}{\partial \theta} = \frac{\frac{1}{A} \cos \theta - \frac{1}{r}}{\frac{r^2}{A^2} - 2 \frac{r}{A} \cos \theta + 1} \quad (C.5)$$

Substituting this relationship into the appropriate equation of eqs. B.6,

$$\frac{\partial \phi}{\partial r} = \frac{\frac{1}{r} - \frac{1}{A} \cos \theta}{\frac{r^2}{A^2} - 2 \frac{r}{A} \cos \theta + 1} \quad (B.7)$$

Eq. B.7 can be integrated to obtain ϕ as follows:

$$\phi = \int \frac{\frac{1}{r} - \frac{1}{A} \cos \theta}{\frac{r^2}{A^2} - 2 \frac{r}{A} \cos \theta + 1} dr$$

$$\phi = A^2 \int \frac{dr}{r(r^2 - 2rA \cos \theta + A^2)} - A \cos \theta \int \frac{dr}{r^2 - 2rA \cos \theta + A^2} \quad (B.8)$$

From the C. R. C. Standard Mathematical Tables (ref. 6),

$$\int \frac{dx}{x(cx^2 + bx + a)} = \frac{1}{2a} \ln \left[\frac{x^2}{cx^2 + bx + a} \right] - \frac{b}{2a} \int \frac{dx}{cx^2 + bx + a}$$

Applied to the first term on the right-hand side of eq. B.8,

(B.9)

$$A^2 \int \frac{dr}{r(r^2 - 2rA \cos \theta + A^2)} = \frac{1}{2} \ln \left[\frac{r^2}{r^2 - 2rA \cos \theta + A^2} \right] + A \cos \theta \int \frac{dr}{r^2 - 2rA \cos \theta + A^2}$$

Substituting eq. B.9 into eq. B.8, the equation for ϕ becomes

$$\phi = \frac{1}{2} \ln \left[\frac{r^2}{r^2 - 2rA \cos \theta + A^2} \right] + f(\theta) \quad (B.10)$$

where the additive $f(\theta)$ term is necessary since the expression is derived by the integration of the partial derivative of ϕ with respect to r .

The evaluation of the $f(\theta)$ term is accomplished by determining $\frac{1}{r} \frac{\partial \phi}{\partial \theta}$ from eq. B.10 and using the resulting expression in the second equation of eqs. B.6. From eq. B.10,

$$\frac{1}{r} \frac{\partial \phi}{\partial \theta} = \frac{-A \sin \theta}{r^2 - 2rA \cos \theta + A^2} + \frac{d[f(\theta)]}{d\theta} \frac{1}{r}$$

Noting that

$$r = A(\cos \theta + \cot \beta \sin \theta)$$

$$\text{and } r^2 = A^2(\cos^2 \theta + 2 \sin \theta \cos \theta \cot \beta + \cot^2 \beta \sin^2 \theta),$$

$$r^2 - 2rA \cos \theta + A^2 = A^2 \sin^2 \theta \csc^2 \beta$$

so that

$$\frac{1}{r} \frac{\partial \phi}{\partial \theta} = -\frac{1}{A} \csc \theta \sin^2 \beta + \frac{1}{r} \frac{d[f(\theta)]}{d\theta} = \frac{\partial \phi}{\partial r}$$

But, from eqs. 3.6,

$$\frac{\partial \beta}{\partial r} = -\frac{1}{A} \csc \theta \sin^2 \beta$$

Consequently,

$$\frac{d[f(\theta)]}{d\theta} = 0$$

$$\text{or } f(\theta) = \text{constant} = \frac{1}{2} \ln \tilde{K}$$

Therefore, ϕ may be written as

$$\phi = \frac{1}{2} \ln \left[\frac{r^2}{r^2 + 2rA \cos \theta + A^2} \right] + \frac{1}{2} \ln \tilde{K}$$

or, finally,

$$\phi = \frac{1}{2} \ln \left[\frac{\tilde{K} r^2}{r^2 - 2rA \cos \theta + A^2} \right] \quad (\text{B.11})$$

Eq. B.11 is the scalar equation for the contours of constant ϕ (the $\nabla \beta$ curves). A more descriptive form of eq. B.11 is obtained by converting to the Cartesian coordinate system. From eq. B.11,

$$e^{2\phi} = \frac{\tilde{K} r^2}{r^2 - 2rA \cos \theta + A^2}$$

$$\text{or } r^2 - 2rA \cos \theta + A^2 = \tilde{K} e^{-2\phi} r^2$$

Therefore,

$$(1 - \tilde{K} e^{-2\phi}) r^2 - 2rA \cos \theta + A^2 = 0$$

$$\text{or } r^2 - \frac{2rA \cos \theta}{(1 - \tilde{K} e^{-2\phi})} + \frac{A^2}{(1 - \tilde{K} e^{-2\phi})} = 0 \quad (\text{B.12})$$

The conversion to Cartesian coordinates is accomplished from eq. B.12 by recognizing that $r^2 = x^2 + y^2$ and $x = r \cos \theta$.

Eq. B.12 becomes

$$x^2 + y^2 - \frac{2A}{(1 - Re^{-2\phi})}x + \frac{A^2}{(1 - Re^{-2\phi})} = 0$$

Completing the square in x and rearranging terms,

$$x^2 - \frac{2A}{(1 - Re^{-2\phi})}x + \frac{A^2}{(1 - Re^{-2\phi})^2} + y^2 = \frac{A^2}{(1 - Re^{-2\phi})^2} - \frac{A^2}{(1 - Re^{-2\phi})}$$

$$\text{or} \quad \left[x - \frac{A}{(1 - Re^{-2\phi})} \right]^2 + y^2 = \frac{A^2}{(1 - Re^{-2\phi})} \left[\frac{1}{(1 - Re^{-2\phi})} - 1 \right] \quad (\text{B.13})$$

Eq. B.13 is in the general form of a circle in the Cartesian coordinate system. Thus, the circular nature of the \vec{v}_β curves in fig. 3-1 is accurate. The radii of the circles are defined by

$$\tilde{R} = A \sqrt{\frac{1}{(1 - Re^{-2\phi})} \left[\frac{1}{1 - Re^{-2\phi}} - 1 \right]} \quad (\text{B.14})$$

and the locations of the centers are

$$(x, y) = \left(\frac{A}{(1 - Re^{-2\phi})}, 0 \right) \quad (\text{B.15})$$

Note that eq. B.15 indicates that the centers of all of the possible circles which are described by eq. B.13 are always on the x - axis of the Cartesian coordinate system (line OQ in fig. B-1).

In order to investigate the acceptability of the second part of assumption "d", the ratio $\frac{\tilde{R}}{\sigma_d}$ must be found. The requirement that the radius of curvature of any particular curve of $\vec{\nabla}\beta$ along which the error is measured is much larger than the one $-\sigma$ error (in distance units) is satisfied if

$$\frac{\tilde{R}}{\sigma_d} \gg 1 \quad (B.16)$$

Since σ_d is still in polar coordinates (eq. B.3), it is convenient to convert \tilde{R} into polar coordinates. From eq. B.11,

$$\tilde{R}e^{-2\phi} = \frac{r^2 - 2rA\cos\theta + A^2}{r^2} \quad (B.17)$$

Substituting $r = A(\cos\theta + \cot\beta \sin\theta)$

and $r^2 = A^2(\cos^2\theta + 2\sin\theta\cos\theta\cot\beta + \cot^2\beta \sin^2\theta)$ into eq. B.17 yields

$$\tilde{R}e^{-2\phi} = \frac{\sin^2\theta \csc^2\beta}{(\cos\theta + \cot\beta \sin\theta)^2}$$

It follows that

$$\frac{1}{(1 - \tilde{R}e^{-2\phi})} = \frac{(\cos\theta + \cot\beta \sin\theta)^2}{\cos 2\theta + \cot\beta \sin 2\theta}$$

$$\text{and } \frac{1}{(1 - \tilde{R}e^{-2\phi})} - 1 = \frac{\sin^2\theta \csc^2\beta}{\cos 2\theta + \cot\beta \sin 2\theta}$$

so that

$$\tilde{R} = A \sqrt{\frac{(\cos\theta + \cot\beta \sin\theta)^2 \sin^2\theta \csc^2\beta}{(\cos 2\theta + \cot\beta \sin 2\theta)^2}}$$

$$\text{or } \tilde{R} = A \sin\theta \csc\beta \left[\frac{\cos\theta + \cot\beta \sin\theta}{\cos 2\theta + \cot\beta \sin 2\theta} \right] \quad (\text{B.18})$$

Dividing eq. B.18 by eq. B.3 yields

$$\frac{\tilde{R}}{\sigma_d} = \frac{1}{(\cos 2\theta + \cot\beta \sin 2\theta) \sigma_a} \quad (\text{B.19})$$

There is an obvious similarity between eq. B.19 for $\frac{\tilde{R}}{\sigma_d}$ and eq. B.4 for $\frac{\hat{R}}{\sigma_d}$. In fact, eq. B.19 can be analyzed as eq. B.4 was for the smallest values of the ratio $\frac{\tilde{R}}{\sigma_d}$ which can be expected by assuming that $\sigma_a = 3 \times 10^{-3}$ radians and setting θ to 45° . Eq. B.19 reduces to

$$\left(\frac{\tilde{R}}{\sigma_d} \right)_\theta = \frac{\pi}{4} = \frac{\tan\beta}{\sigma_a} = (3.3 \times 10^2) \tan\beta \quad (\text{B.20})$$

Fig. B-3 illustrates eq. B.20 for $0 \leq \beta \leq 50^\circ$. If $\frac{\tilde{R}}{\sigma_d} \geq 10$ is considered sufficient to satisfy eq. B.16, it can be seen from the figure that the second part of assumption "d" is acceptable if $\beta \geq 1^\circ 43'$. Therefore, the linearity of the curves of $\frac{\tilde{R}}{\sigma_d}$ in the neighborhood of P for any value of θ corresponding to essentially all the possible values of β is acceptable; and the second part of assumption "d" is generally acceptable.

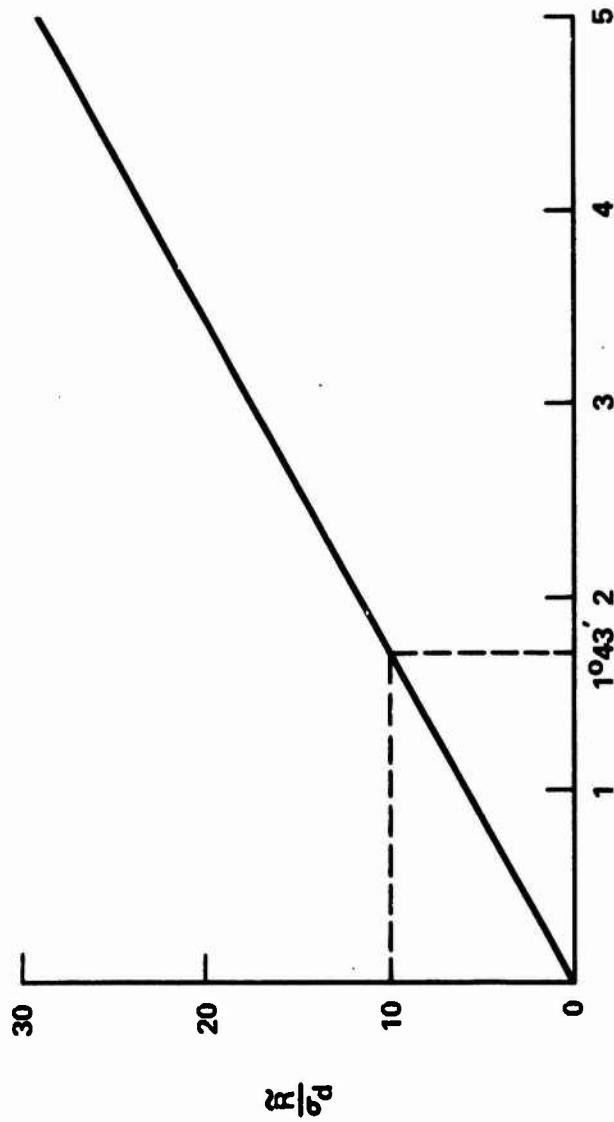


Figure B-3. Graphic Representation of Equation B.20 for $0 \leq \beta \leq 5^\circ$

APPENDIX C

This appendix contains the derivation of eq. 3.8 from eq. 3.4.
Eq. 3.4 is restated for convenience as

$$\beta = \cot^{-1} \left[\frac{r}{A} \csc \theta - \cot \theta \right] \quad (3.4)$$

In polar coordinates,

$$\vec{\nabla} \beta = \frac{\partial \beta}{\partial r} \hat{r} + \frac{1}{r} \frac{\partial \beta}{\partial \theta} \hat{\theta} \quad (3.5)$$

The components of $\vec{\nabla} \beta$ are calculated as follows:

$$\frac{\partial \beta}{\partial r} = \frac{-\frac{1}{A} \csc \theta}{\frac{r^2}{A^2} \csc^2 \theta - 2 \frac{r}{A} \csc \theta \cot \theta + \cot^2 \theta + 1} \quad (C.1)$$

Using the trigonometric identity $\csc^2 \theta = \cot^2 \theta + 1$, eq. C.1 becomes,

$$\frac{\partial \beta}{\partial r} = \frac{-\frac{1}{A} \csc \theta}{\csc^2 \theta \left(\frac{r^2}{A^2} - 2 \frac{r}{A} \cos \theta + 1 \right)}$$

It follows that

$$\frac{\partial \beta}{\partial r} = \frac{-\frac{1}{A} \sin \theta}{\frac{r^2}{A^2} - 2 \frac{r}{A} \cos \theta + 1} \quad (C.2)$$

Finally, substituting

$$r = A(\cos \theta + \cot \beta \sin \theta) \quad (C.3)$$

$$\text{and } r^2 = A^2(\cos^2 \theta + 2 \sin \theta \cos \theta \cot \beta + \cot^2 \beta \sin^2 \theta)$$

into C.2 and combining terms,

$$\frac{\partial \beta}{\partial r} = -\frac{1}{A} \csc \theta \sin^2 \beta \quad (C.4)$$

$$\frac{\partial \beta}{\partial \theta} = \frac{\frac{r}{A} \csc^2 \theta \cos \theta - \csc^2 \theta}{\csc^2 \theta \left(\frac{r^2}{A^2} - 2 \frac{r}{A} \cos \theta + 1 \right)}$$

$$\frac{1}{r} \frac{\partial \beta}{\partial \theta} = \frac{\frac{1}{A} \cos \theta - \frac{1}{r}}{\frac{r^2}{A^2} - 2 \frac{r}{A} \cos \theta + 1} \quad (C.5)$$

Substituting eqs. C.3 into eq. C.5 and combining terms,

$$\frac{1}{r} \frac{\partial \beta}{\partial \theta} = \frac{\cos^2 \theta + \sin \theta \cos \theta \cot \beta - 1}{A \sin^2 \theta \csc^2 \beta (\cos \theta + \cot \beta \sin \theta)}$$

$$\text{or } \frac{1}{r} \frac{\partial \beta}{\partial \theta} = -\frac{1}{A} \csc \theta \sin^2 \beta \left[\frac{\sin \theta - \cot \beta \cos \theta}{\cos \theta + \cot \beta \sin \theta} \right] \quad (C.6)$$

The magnitude of $\vec{\nabla} \beta$, given by eq. 3.7, is restated here for convenience.

$$|\vec{\nabla} \beta| = \sqrt{\left(\frac{\partial \beta}{\partial r} \right)^2 + \left(\frac{1}{r} \frac{\partial \beta}{\partial \theta} \right)^2} \quad (3.7)$$

Using the expressions of eqs. C.4 and C.6 in eq. 3.7,

$$|\vec{\nabla} \beta| = \frac{1}{A} \csc \theta \sin^2 \beta \sqrt{1 + \left[\frac{\sin \theta - \cot \beta \cos \theta}{\cos \theta + \cot \beta \sin \theta} \right]^2}$$

Expanding the expression under the radical and combining terms yields

$$|\vec{\nabla}_\beta| = \frac{\csc\theta \sin\beta}{A(\cos\theta + \cot\beta \sin\theta)} \quad (3.8)$$

APPENDIX D

This appendix presents the derivation of the expression for $\left. \frac{\partial \text{GMOP}}{\partial \beta} \right|_0$, eq. 3.15, from eq. 3.9. To begin, eq. 3.9 is restated for convenience.

$$\text{GMOP} = \frac{1}{A \left| \frac{\partial \beta}{\partial \theta} \right|} = \sin \theta \csc \beta (\cos \theta + \cot \beta \sin \theta) \quad (3.9)$$

$$\left. \frac{\partial \text{GMOP}}{\partial \beta} \right|_0 = - \sin \theta \cot \beta \csc \beta (\cos \theta + \cot \beta \sin \theta) - \sin^2 \theta \csc^3 \beta$$

Expanding and manipulating,

$$\left. \frac{\partial \text{GMOP}}{\partial \beta} \right|_0 = - \sin \theta \cos \theta \cos \beta \csc^2 \beta - \sin^2 \theta \cos^2 \beta \csc^3 \beta - \sin^2 \theta \csc^3 \beta$$

Factoring and using $\cos^2 \beta = 1 - \sin^2 \beta$,

$$\left. \frac{\partial \text{GMOP}}{\partial \beta} \right|_0 = - \sin \theta \csc^2 \beta \left[\cos \theta \cos \beta + \sin \theta \csc \beta (2 - \sin^2 \beta) \right]$$

or

$$\left. \frac{\partial \text{GMOP}}{\partial \beta} \right|_0 = - \sin \theta \csc^2 \beta \left[\cos \theta \cos \beta + 2 \sin \theta \csc \beta - \sin \theta \sin \beta \right]$$

Noting that $\cos(\beta + \theta) = \cos \theta \cos \beta - \sin \theta \sin \beta$,

$$\left. \frac{\partial \text{GMOP}}{\partial \beta} \right|_0 = - \sin \theta \csc^2 \beta \left[\cos(\beta + \theta) + 2 \sin \theta \csc \beta \right]$$

and, finally,

$$\left. \frac{\partial \text{GMOP}}{\partial \beta} \right|_0 = - \sin \theta \csc^3 \beta \left[\sin \beta \cos(\beta + \theta) + 2 \sin \theta \right] \quad (3.15)$$